photonics

MDPI

Review

Applying Quantum Cascade Laser Spectroscopy in Plasma Diagnostics

Jürgen Röpcke [1,*], Paul B. Davies [2], Stephan Hamann [1], Mario Hannemann [1], Norbert Lang [1] and Jean-Pierre H. van Helden [1]

[1] Leibniz Institute for Plasma Science and Technology (INP Greifswald), Felix-Hausdorff-Str. 2, 17489 Greifswald, Germany; hamann@inp-greifswald.de (S.H.); hannemann@inp-greifswald.de (M.H.); lang@inp-greifswald.de (N.L.); jean-pierre.vanhelden@inp-greifswald.de (J-P.H.v.H.)

[2] Department of Chemistry, University of Cambridge, Lensfield Road, Cambridge CB2 1EW, UK; pbd2@cam.ac.uk

* Correspondence: roepcke@inp-greifswald.de; Tel.: +49-3834-554-444

Received: 22 June 2016; Accepted: 21 July 2016; Published: 25 July 2016

Abstract: The considerably higher power and wider frequency coverage available from quantum cascade lasers (QCLs) in comparison to lead salt diode lasers has led to substantial advances when QCLs are used in pure and applied infrared spectroscopy. Furthermore, they can be used in both pulsed and continuous wave (cw) operation, opening up new possibilities in quantitative time resolved applications in plasmas both in the laboratory and in industry as shown in this article. However, in order to determine absolute concentrations accurately using pulsed QCLs, careful attention has to be paid to features like power saturation phenomena. Hence, we begin with a discussion of the non-linear effects which must be considered when using short or long pulse mode operation. More recently, cw QCLs have been introduced which have the advantage of higher power, better spectral resolution and lower fluctuations in light intensity compared to pulsed devices. They have proved particularly useful in sensing applications in plasmas when very low concentrations have to be monitored. Finally, the use of cw external cavity QCLs (EC-QCLs) for multi species detection is described, using a diagnostics study of a methane/nitrogen plasma as an example. The wide frequency coverage of this type of QCL laser, which is significantly broader than from a distributed feedback QCL (DFB-QCL), is a substantial advantage for multi species detection. Therefore, cw EC-QCLs are state of the art devices and have enormous potential for future plasma diagnostic studies.

Keywords: plasma diagnostics; quantum cascade laser; infrared spectroscopy

1. Introduction

Over the last two decades, chemical sensing using mid infrared laser absorption spectroscopy (MIR-LAS) in the molecular fingerprint region from 3 to 20 μm, which contains strong ro-vibrational absorption bands of a large variety of gaseous species, has been established as a powerful in situ diagnostic tool for molecular plasmas [1–6]. Quantum cascade lasers (QCL) in particular have played a central role in this field so much so that they have become the infrared light sources of choice for plasma diagnostics in the mid infrared. The methods of MIR-LAS provide a means of detecting stable and transient molecular species in ground and excited states and of measuring the concentrations and temperatures of reactive species in plasmas. Compared to "pure" trace gas detection, e.g., in environmental and combustion studies, high sensitivity is not the only issue for plasma diagnostic applications. Since kinetic processes are inherent to discharges ignited in molecular gases, high time resolution on sub millisecond timescales is frequently desired for fundamental studies as well as for process monitoring in applied research and industry. In addition to high sensitivity and good temporal

resolution the capacity for broad spectral coverage enabling multi-component detection encompassing molecules with broader absorption structures is further expanding the use of MIR-LAS techniques. QCLs possess all above mentioned characteristics required for MIR-LAS as will be demonstrated by the examples described in detail later on.

Tunable diode laser absorption spectroscopy (TDLAS) in the mid infrared spectral region using lead salt lasers light sources has proven to be a versatile diagnostic technique for molecular plasmas [7–10]. However, lead salt lasers are beset by several limitations in particular short isolated spectral modes and low power. A further disadvantage of lead salt diode lasers as light sources is the necessity for cooling of both the lasers and the detectors which operate at temperatures below 100 K. Systems based on lead salt diode lasers therefore require bulky closed cycle refrigerators and/or cryogens like liquid nitrogen [11,12].

The development and commercial availability of pulsed and continuous wave (cw) QCLs for wavelengths longer than 3.4 μm and interband cascade lasers (ICLs) for shorter wavelengths has stimulated very significant improvements in MIR-LAS for plasma diagnostic purposes. The first QCL devices could only be used at room temperature in pulsed mode with low duty cycles. Room temperature cw lasers became available following the successful solution of heat dissipation problems [13,14]. Compared to lead salt lasers, distributed feedback (DFB) QCLs provide (i) continuous mode-hop free (MHF) wavelength tuning; (ii) increasingly high output powers up to hundreds of mW; (iii) room temperature operation, and in the case of cw DFB-QCLs; (iv) narrow linewidth radiation. The emission wavelength of this new class of thermoelectrically (TE) cooled semiconductor lasers can be tailored over a wide wavelength range throughout the infrared molecular fingerprint region. The total emission range of a single DFB-QCL is typically less than 7 cm^{-1} (see [2] and references therein). Therefore, multi-component detection to study infrared active compounds in reactive plasmas and gases requires, as in the case of TDLAS, the combination of several QCLs in a spectrometer [15,16]. Nevertheless, the variety of QCLs and ICLs operating at room temperature provide alternatives to cryogenically cooled lead salt lasers. Fortunately, tunability over much broader spectral ranges than possible with a typical lead salt laser or DFB-QCL has been achieved using external cavity (EC) QCLs. EC-QCLs are state of the art devices already in use in an increasing number of applications including high resolution isotope analysis, explosive detection and trace gas monitoring [17–22]. Nowadays, EC-QCLs, which work in pulsed or cw modes, can be tuned over more than 100 cm^{-1}. Currently available cw EC-QCLs provide MHF tuning ranges as large as 80 cm^{-1} and powers up to 350 mW [2]. Further extension of tuning ranges and even higher laser powers have been achieved in specific cases [17].

Broadly speaking, the commercial availability of different types of DFB- and EC-QCLs along with their convenient operating conditions and performance has led to the rapid development of MIR-LAS from a niche position to a standard diagnostic technique [3,6]. A topical review on the application of MIR-LAS in plasma diagnostics was published in 2012 [6]. The present article is intended as an extension of that paper compiling recent achievements and modern trends in the rapidly changing field of plasma spectroscopy. The 31 papers published in this field between 2006 and 2012, already discussed in reference [6], together with 18 new plasma diagnostic applications of mid infrared QCLs published since 2013, are compiled in Table 1.

The article is subsequently divided into three main sections: Section 2 starts with the spectroscopic issues usually encountered with pulsed QCLs. These lasers are frequently employed for a wide variety of applications including studies with very high time resolution. Special attention is devoted to in situ studies of plasma chemistry and reaction kinetics in gas discharges and on selected aspects of plasma surface interactions. A link is thereby provided to modelling of plasmas and surface phenomena. Additionally, the current status of industrial process monitoring in the mid infrared is reviewed. Section 3 concerns the application of cw QCLs and Section 4 focuses on the current status and the potential of advanced instrumentation based on EC-QCLs for plasma diagnostic applications.

Table 1. Plasma diagnostic applications of mid infrared (MIR) quantum cascade lasers (QCLs).

Species	Spectral Range (cm^{-1})	Type of Plasma	Application [1]	Pressure (mbar) [2]	Type of QCL	Tuning Method	Method of Absorpt [3]	Time Resolution	Year	Ref.
CH_4	~1275	MW	Res.	>50	pulsed	intra	DAS/SP	1 s	2006	[23]
NO	1897	DC	Res.	2.7	pulsed	intra	DAS/SP	5 µs	2007	[24]
SiF_4	1028	RF	Ind.	0.33	pulsed	inter	DAS/DP	~1 s	2007	[25]
CH_4	1253	RF	Res.	0.23	pulsed	intra	DAS/SP	n.a.	2008	[26]
CF_3	1253	Photolysis	Res.	2.6 ... 5.4	pulsed	intra	DAS/SP	5 µs	2008	[27]
C_2H_2	~1275	Flame	Res.	1013	pulsed	intra	DAS/SP	n.a.	2009	[28]
NF_3	1028	RF	Ind.	0.33	pulsed	inter	DAS/DP	~1 s	2009	[29]
C_2H_2	~1275	MW	Res.	199.5	pulsed	intra	DAS/SP	1 s	2009	[30]
SiH_4	2244	VHF [4]	Res. (Ind.)	3.5 ... 4.5	cw		DAS/SP	n.a.	2009	[31]
BCl_3	964	MW	Res.	2	pulsed	inter	DAS/DP	3 s	2009	[32]
NO	1900	DPBPR [5]	Res.	1013.25	cw		DAS/SP	>1 s	2009	[33]
CF_4 C_3F_8	1271 1274	RF	Res.	0.1	pulsed	intra	DAS/DP	5 ms	2009 2010	[34–36]
SiF_4 C_4F_6	1028 973	MW	Res. (Ind.)	0.2 ... 0.3	pulsed pulsed	inter	DAS/DP	1 s	2010	[37]
CH_4	1303	MW	Res.	1.5	cw		DAS/SP	0.2 s	2010	[3]
HCN	1304	MW	Res.	1.5	cw		CEAS	>1 s	2010	[3]
NO	1819	MW	Res.	1.5	cw		CEAS	>1 s	2010	[3]
BCl_3	964	DC	Ind.	2	pulsed	inter	DAS/DP	3 s	2010	[38]
NO NO_2	1897 1612	RF	Res.	0.53	pulsed	intra	DAS/SP	>1 s	2010	[5]
CH_4	1343	RF	Res.	0.1	pulsed	inter	DAS/DP	>1 s	2010	[39]
C_2H_2	1344	RF	Res.	0.055	pulsed	inter	DAS/DP	>1 s	2011	[40]
CO COF_2 SiF_4	2078 ? 1031	ICP-RF	Ind.	0.009	pulsed	inter	DAS/MP	>1 s	2011	[41]
BCl_3	9635	DC	Ind.	2	pulsed	inter	DAS/SP	<1 s	2011	[42]
N_2O NO NO_2	2207 1900 1615	DC	Res.	1.33	pulsed	intra	DAS/SP	<1 µs	2011	[15]

Table 1. *Cont.*

Species	Spectral Range (cm^{-1})	Type of Plasma	Application [1]	Pressure (mbar) [2]	Type of QCL	Tuning Method	Method of Absorpt [3]	Time Resolution	Year	Ref.
CH_4 C_2H_2	1343 1344	ICP-RF	Res.	0.43	pulsed	inter	DAS/MP	>1 s	2011	[43]
NO NO_2	1897 1612	DC	Res.	0.53	pulsed	intra	DAS/SP	>1 s	2011	[44]
NO	1897	DC	Res.	2.66	pulsed	intra	DAS/DP	<1 µs	2011	[45]
CO_2	2325	DC	Res.	1.33	pulsed	intra	DAS/DP	<1 µs	2012	[46]
O_3	1027	VHF [4]	Res.	1013.25	pulsed	inter	DAS/MP	>1 s	2012	[47]
CH_4 C_2H_2 C_2H_4 H_2O HCN HNO_3	1333 1333 1413 1375 1383 1333	RF	Res.	0.06	EC		DAS/MP	>1 s	2012	[48]
CH_4 C_2H_2 H_2O HCN	1381 1333 1375 1383	MW	Res.	0.5	EC		DAS/MP	>1 s	2012	[49]
NO	1900	DC	Res.	1.33	pulsed		DAS/DP	<1 µs	2012	[50]
C_2H_2 CO CO_2	1345 2206 2329	DC	Res.	2.6	pulsed	intra	DAS/DP	>1 s	2013	[51]
CO CO_2 N_2O	2143 2349 2224	DC	Res.	1.33	pulsed	intra	DAS/DP	<1 µs	2013	[52]
NO_2	1641	VHF [4]	Res.	1013.25	pulsed	ATTC [6]	DAS/SP	<1 µs	2013	[53]
NO_2	1612	VHF [4]	Res.	1013.25	pulsed	inter	DAS/MP	>1 s	2014	[54]
CH_4 C_2H_2	1347	VHF [4]	Res.	0.003	cw		DAS/MP	>1 s	2014	[55]
O_3	1027	VHF [4]	Res.	1013.25	pulsed	inter	DAS/MP	>1 s	2015	[56]
SiH_4	2244	VHF [4]	Res. (Ind.)	3.5 ... 4.5	cw		DAS/SP	n.a.	2015	[57]

Table 1. *Cont.*

Species	Spectral Range (cm^{-1})	Type of Plasma	Application [1]	Pressure (mbar) [2]	Type of QCL	Tuning Method	Method of Absorpt [3]	Time Resolution	Year	Ref.
CO SiF_4	2078 1031	ICP-RF	Ind.	0.009	pulsed	inter	DAS/MP	>1 s	2015	[58]
CF_2	1106	ICP-RF	Ind.	0.0133	cw		DAS/MP	<1 s	2015	[59]
O_3 NO_2	1027 1612	VHF [4]	Res.	1013.25	pulsed	inter	DAS/MP	>1 s	2015	[60]
O_3 NO_2	1027 1612	VHF [4]	Res.	1013.25	pulsed	inter	DAS/MP	>1 s	2015	[61]
CH_4 C_2H_2 HCN NH_3	1356 1357 1388 1388	DC	Res.	3	EC		DAS/MP	>1 s	2015	[62]
CH_4 C_2H_2 HCN NH_3	1356 1357 1388 1388	DC	Res.	3	EC		DAS/MP	>1 s	2015	[63]
NO NO_2 N_2O	2207 1900 1615	DC	Res.	1.33	pulsed	intra	DAS/DP	<1 µs	2016	[64]
NO N_2O	1903 2213	RF	Res.	1013.25	pulsed	intra	DAS/MP	<1 µs	2016	[65]
CO	2197	MW	Res.	0.25–0.55	EC		DAS/MP	<1 s	2016	[66]
CO	2197	MW	Res.	0.25–0.55	EC		DAS/MP	<1 s	2016	[67]
CO	2147	MW	Res.	0.25–0.5	EC		DAS/MP	<1 s	2016	[68]

[1] Res. = research environment, Ind. = industrial application; [2] converted into mbar, if necessary; [3] DAS = direct absorption spectroscopy, SP = single pass, DP = double pass, MP = multi-pass; [4] VHF = very high frequency; [5] DPBPR = dielectric packed bed plasma reactor; [6] ATTC = amplitude-to-time conversion

2. Application of Pulsed QCLs in Low- and Atmospheric Pressure Plasmas

2.1. General Spectroscopic Issues

The first QCL devices were typically characterized by low efficiency, i.e., the portion of electrical input power that was converted into radiation, was of the order of a few percent and QCLs were thus mainly producing heat. This hampered cw lasing at room temperature for a long time and required pulsed operation for commercially available devices to work. Initial experiments with pulsed QCLs combined short laser pulses of the order of a few nanoseconds with the same method used for scanning TDLs, namely adding a sub-threshold DC current ramp [69]. This was called the *inter pulse* mode. In this mode, the spectral tuning is performed by temperature induced changes of the refractive index of the laser which tunes both the spectral gain and to a lesser extent the characteristics of the DFB grating [70]. In contrast to lead salt lasers, QCLs require up to an order of magnitude higher compliance voltages and considerably increased input power to the laser. This in turn makes the device's temperature vary and consequently its refractive index, particularly during a laser pulse. As a result, an inherent frequency-down chirp is observed for pulsed QCLs. This was later advantageously exploited by using single long laser pulses (i.e., some hundred nanoseconds) to acquire entire absorption spectra in a very short time scale. This quantum cascade laser absorption spectroscopy (QCLAS) method is known as the *intra pulse* mode [71,72]. From the middle of the last decade QCLAS has been successfully implemented for a variety of plasma diagnostics purposes (see [3] and references therein), although specific obstacles such as pulse-to-pulse fluctuations inherent to pulsed operation had to be overcome. Recently, the so called intermittent operation of cw QCLs, using a rectangular pulse for tuning, has been proposed [73].

In addition, spectral line broadening effects were identified as the main challenge when using the *inter pulse or intra pulse* mode for highly sensitive detection schemes [74,75]. Effective laser line widths (full width at half maximum—FWHM) between 0.0095 cm^{-1} (290 MHz) and 0.093 cm^{-1} (2.79 GHz) have been reported. McCulloch and co-authors deduced that the spectral resolution of QCL spectrometers is determined both by the chirp rate and the pulse width of the lasers [75]. While short pulse spectrometers may approach the Fourier limit for extremely short pulses of the order of 5 ns [76] increased pulse widths lead to a chirp limited resolution (70 ns, 2.79 GHz [77]). Furthermore, several studies reported observing absorption features with asymmetric line shapes when employing both the short pulse and the long pulse mode (see [3] and references therein). Additionally, the latter method suffers from non-linear absorption effects [78]. The majority of these issues are unknown in using cw QCLs and degrade the performance of pulsed QCL spectrometers. This is of particular importance at lower pressures, since under such conditions the effective laser line width of pulsed QCLs exceeds the typical Doppler line broadening. Non-linear effects also appeared more pronounced [26,78].

Recently, Welzel et al. have carried out a comparative study of non-symmetrical line broadening effects with sub-nanosecond time resolution using a short-pulse QCL spectrometer and a conventional TDL set-up [79]. This two laser arrangement consisting of co-aligned TDL and QCL spectrometers. Flip mirrors were used to switch between the systems. Artefacts in the recorded spectra such as irregular line shapes or poorly determined (underestimated) absorption coefficients were reported based on a detailed time-resolved high-bandwidth analysis of individual pulses during a laser sweep. The origin of the artefacts using short pulses (*inter pulse* mode) was identified as partly of the same nature as in the case of long laser pulses (*intra pulse* mode). Quantitative results for CH_4 absorption features fell short of the expected values. The nominal mixing ratio (=1) was confirmed by using TDLAS. An apparent increased instrumental broadening, i.e., of the effective line width of the QCL, and underestimated concentrations under low pressure conditions were found to be attributable to the complex tuning characteristics. These effects appeared more pronounced at higher laser intensities, i.e., well above threshold, and for strong absorption features [79].

A compilation of the main spectroscopic issues encountered when using pulsed QCLs for plasma diagnostic purposes has been given in reference [3]. In particular, under low pressure conditions, non-linear absorption effects may appear. As a consequence, correction or calibration procedures for measuring reliable concentration values have to be considered [24,26].

2.2. Methods for Determining Gas Temperatures in Plasmas

In plasma physics, plasma chemistry and also in plasma technology the gas temperature is a very important parameter, since the rate coefficients of chemical reactions in the gas volume, the diffusion of gaseous species and also heterogeneous reactions on surfaces usually show a strong dependence on the temperature [80]. Even in a monoatomic gas, the plasma density distribution cannot be calculated without knowledge of the temperature distribution. The determination of the gas temperature by emission and absorption spectroscopy is quite common in plasma diagnostics. For example, the measurement of the Doppler broadening of spectral lines is a well known and widely used method of temperature determination. Nevertheless, the implementation of the method is not that simple in practice, because the main problems are: (i) the determination of the instrumental function of the spectrometer; (ii) taking into account the multiplet and fine structure of lines; and (iii) extraction of the Doppler broadening contribution from the measured line profile while (iv) considering possible pressure broadening and line profile distortion effects.

An alternative spectroscopic approach is the analysis of rotational temperatures of molecules in excited ro-vibrational states. Here, the rotational temperature has definite physical meaning if the time of rotational relaxation in a certain vibronic state is much smaller than the mean lifetime of the rotational levels. In this case, the rotational distribution of the populations is close to a Boltzmann distribution, with the temperature equal to the translational temperature of the colliding particles; see reference [81] and references therein.

In particular, MIR-LAS using lead salt lasers or quantum cascade lasers is a valuable technique to study ro-vibrational transitions of molecules in plasmas. Already in 1998, Allen described a method employing the intensity ratios of measured absorption lines [82]. A spectrometer based on lead salt lasers was applied to determine rotational temperature values, which were shown to be in good agreement with the gas temperature. Both methods, TDLAS and QCLAS, can be used as a non-invasive temperature probe. A time resolution approaching the sub-microsecond time scale can be achieved when pulsed QCLs are applied [80]. This high temporal resolution will improve the understanding of kinetic processes in, e.g., pulsed plasmas on line and in situ.

An example for such measurements is provided in Figures 1–4. A pulsed DC air plasma admixed with 0.8% NO was studied in a Pyrex tube reactor. A time resolution of 33 µs was provided by the QCLAS system. Figure 1 presents the main features of the optical set-up. The Pyrex tube was 60 cm in length with an inner diameter of 20 mm. The pulsed QCL was aligned to achieve three passes through the tube and the line ratio method was applied to determine the gas temperature. For this purpose, the temperature dependent intensity ratio of two absorption features of NO at 1900 cm^{-1} (5.26 µm) was used. Figure 2 shows the NO spectrum detected in the time domain. The time axis has been calibrated to fit to the wavenumber axis. The QCLAS system was operated in the *intra pulse* mode with a pulse repetition frequency of 30 kHz leading to an entire spectrum every 33 µs. As a typical result for a 150 mA plasma pulse the calculated temporal evolution of the temperature of NO diluted in air is shown in Figure 3. Different mean plasma currents have been applied to the discharge leading to gas temperature between 300 K and 500 K, (Figure 4) [50].

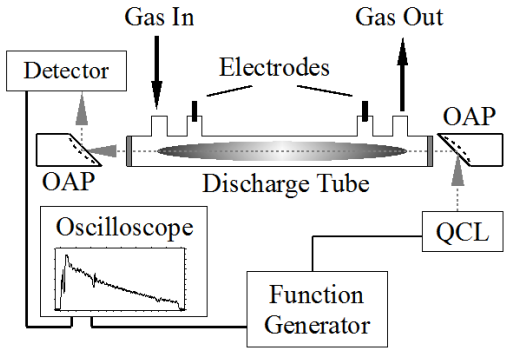

Figure 1. Principal sketch of the optical set-up used for temperature determination. The radiation of the QCLAS system was passed three times through the Pyrex discharge cell. The cell was 60 cm in length with an inner diameter of 20 mm. The experiments were performed under static gas conditions, $P_{initial}$ = 1.33 mbar [50], © IOP Publishing. Reproduced with permission. All rights reserved.

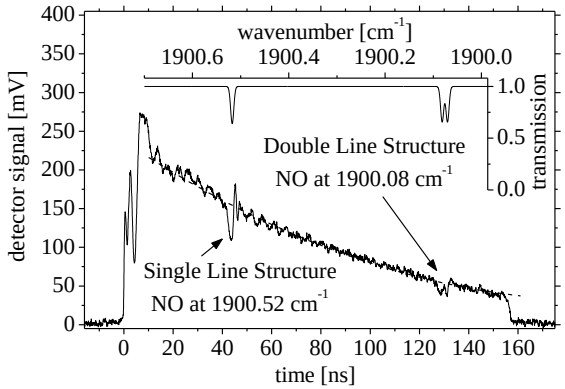

Figure 2. Detected NO spectrum in the time domain measured by the QCLAS system. The spectrum (solid line) corresponds to 0.8% NO in air at a pressure of 1.33 mbar with an absorption length L = 180 cm. The dashed curve shows the baseline. The embedded diagram shows a simulated NO spectrum using the HITRAN database [50,83], © IOP Publishing. Reproduced with permission. All rights reserved.

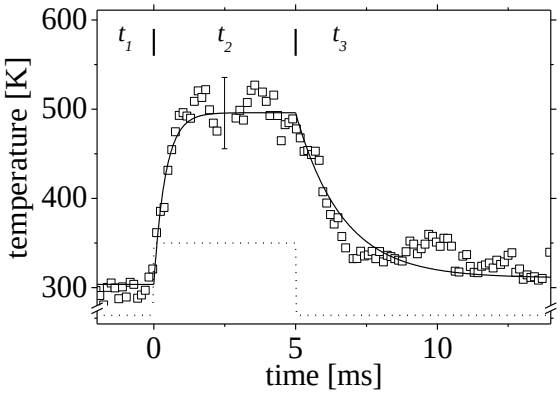

Figure 3. Calculated temporal evolution of the temperature of NO diluted in air (symbols) for a 150 mA plasma pulse. Exponential functions have been fitted to the temperature rise during the pulse, t_2, as well as to the cooling period after the plasma pulse, t_3 [50], © IOP Publishing. Reproduced with permission. All rights reserved.

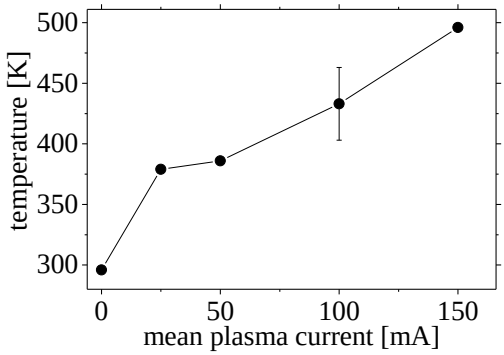

Figure 4. Calculated gas temperatures during the plasma pulse as a function of the mean plasma current. The total pressure of the gas mixture containing 0.8% NO in air was 1.33 mbar [50], © IOP Publishing. Reproduced with permission. All rights reserved.

2.3. Study of Plasma Surface Interactions in Low-Pressure Plasmas

2.3.1. On the Reactivity of Plasma Treated Photo-Catalytic TiO_2 Surfaces for Oxidation of C_2H_2 and CO

Over the past decade, the approach of combining plasmas with catalysts has been a technical as well as a scientific challenge for improved pollutant destruction. Plasma-catalyst synergy has been studied in air discharges with admixtures of volatile organic compounds using different types of catalysts at atmospheric and sub-atmospheric pressures [84–88]. One of the main issues of plasma-catalyst coupling is understanding the interaction of the plasma with the catalytic material, especially the processes involved in the production and destruction of molecules on the wall. This field is only just beginning to become more intensively analyzed due to the great complexity of the physical and chemical phenomena occurring at atmospheric pressure. A useful alternative to understanding the specific aspects of plasma-catalytic surface interaction is to perform studies at lower pressure, where surface reactions are dominant over gas phase reactions. This also provides an original route for performing time resolved diagnostics of surface reactivity [51].

Based on this approach the reactivity of plasma treated and plasma stimulated TiO_2 catalytic surfaces have been studied by analyzing the oxidation of (i) C_2H_2 to CO and CO_2 and (ii) CO to CO_2. The inner surface of a Pyrex discharge tube, shown in Figure 5, was coated with TiO_2 films impregnated with TiO_2 nano-particles, which provided a surface area of about 4 m^2. In addition to the exposure of the TiO_2 surface to low pressure RF plasmas using O_2, Ar or N_2 (f = 13.56 MHz, p = 0.53 mbar, P = 17 W) the surfaces have also been activated by heating and UV radiation treatment.

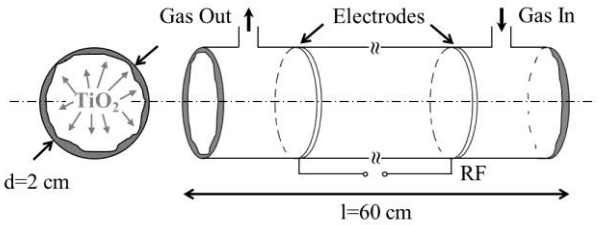

Figure 5. Schematic of the Pyrex tube coated internally with a TiO_2 sol-gel film and TiO_2 nano-particles, with two electrodes, placed outside the tube [51], © IOP Publishing. Reproduced with permission. All rights reserved.

A clean inner tube surface was ensured by following a rigorous cleaning procedure before each measurement, which included heating to 350 °C, UV irradiation and O_2 plasma treatment for about 50 min. This pre-treatment procedure ensured that any memory effect of the tube surface was eliminated and hence a high level of reproducibility was achieved.

The experimental details are given in Table 2. The temporal evolution of the experiments consisted of four main phases: (1) pre-treatment; (2) evacuation; (3) filling and adsorption; and (4) post treatment. Phase 1 is divided into three alternative sub-phases: (i) O_2 or (ii) N_2 or (iii) Ar plasma. While phase 4 is characterized by two alternative sub-phases: (i) heating to 350 °C or (ii) UV radiation.

Table 2. Experimental phases of the measurements [51], © IOP Publishing. Reproduced with permission. All rights reserved.

Phase No.	**1**			**2**	**3**	**4**	
Phase Name	Pre-Treatment (Plasma Activation)			Evacuation	Filling and Adsorption	After-Treatment (Stimulated Oxidation)	
Sub-Phase Name						Heating 350 °C	UV radiation
Precursor Gas	O_2	N_2	Ar		1% C_2H_2 or 1% CO in Ar	Ar Buffer	
Pressure (mbar)	1.25	0.75	0.26	Pumping	1.3–6.6	2.6	
Duration (min)	10–30	10–30	10–20	10	5–30	25	35
Flowing (FC) or Static (SC) Conditions	FC	FC	FC		SC	SC	

The pre-treatment, phase 1, is used for the deposition of oxygen atoms, O_{ads}, on the inner TiO_2 surface via exposure to a pure O_2 plasma for 10–30 min [89]. To verify the effect of the O_2 plasma, in some specific experiments an Ar or N_2 plasma was used. Following this pre-treatment phase, in phase 2 the tube was pumped for 10 min to evacuate all gaseous species and to allow the tube to cool down to room temperature. After pre-treatment and pumping, in phase 3 the tube was filled with the relevant probing gas containing either C_2H_2 or CO. At the same time, the in situ monitoring of the temporal evolution of the concentrations of C_2H_2, CO and CO_2 using QCLAS was started under static conditions. In phase 4, an after-treatment was applied to activate the TiO_2 catalyst either by heating (350 °C) or by UV radiation.

Following pre-treatment with Ar or N_2 discharges, using an initial gas mixture of 1% C_2H_2 in Ar, the C_2H_2 concentration was found to be nearly constant over time, on the other hand a strong decay in the concentration of C_2H_2 was observed for pure O_2 plasma pre-treatment. In general, the decay was found to be nearly exponential with a time constant of the order of 10 min. The time evolution of the concentrations of C_2H_2 and of CO_2 in phases 3 and 4 is shown in Figure 6.

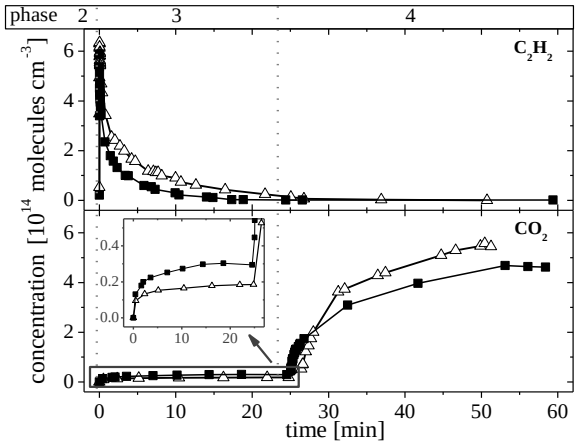

Figure 6. Time evolution of the concentrations of C_2H_2 (upper panel) and of CO_2 (lower panel) in phases 3 and 4 (initial gas mixture: 1% C_2H_2 in Ar, p = 2.6 mbar). After-treatment: Δ—heating to 350 °C and ■—UV radiation exposure [51], © IOP Publishing. Reproduced with permission. All rights reserved.

A relatively small production of CO_2, on the order of 10^{13} molecules cm^{-3}, was observed during the adsorption of C_2H_2 on the stimulated TiO_2 surface, see inset of Figure 6. The concentration of CO_2 grew slowly and after 20–25 min reached a value of nearly 2–3 $\times$ 10^{13} molecules cm^{-3}. This represents only about 2% of the carbon provided from the consumed acetylene. The reactive adsorption of C_2H_2 molecules on the inner surface of the tube reactor showed a density of about 7.5 $\times$ 10^{12} C_2H_2 molecules cm^{-2}.

After the C_2H_2 concentration has stabilized the reactor contains mainly argon as buffer gas at a pressure of p = 2.6 mbar. Therefore, to initiate oxidation reactions the catalyst was activated in two possible ways: (i) by heating to 350 °C or (ii) by exposure to UV radiation, phase 4. It should be pointed out that no C_2H_2 desorption had been seen, when the catalyst was heated. This fact confirms the reactive mechanism of the adsorption process. If acetylene had been just molecularly adsorbed, a thermally initiated desorption of C_2H_2 would be observed.

This behavior demonstrates that the reaction $(O_{ads} + C_2H_2)_{TiO2}$ produces some adsorbed intermediates, which can be thermally or photo-catalytically oxidized to CO_2. In contrast, when 1% CO in Ar was used as the initial gas mixture no adsorption processes on the TiO_2 surface was detected. Figure 7 compares the photo-catalytic decomposition (i) of CO and the formation of CO_2 in phases 3 and 4 after an Ar plasma pre-treatment in phase 1 and (ii) the decomposition of CO and formation of CO_2 after an O_2 plasma pre-treatment in phase 1. In the case where the pre-treatment in phase 1 was performed with an O_2 plasma, the CO destruction in phase 4 via the UV exposure of the photo-catalytic TiO_2 layer is much more effective. In contrast to the case of C_2H_2 no reduction of the CO concentration in phase 3 was observed. However, in the case of an O_2 plasma pre-treatment with UV stimulation, an effective CO oxidation and CO_2 production takes place. Within just a few minutes nearly all the CO molecules have been oxidized (Figure 7).

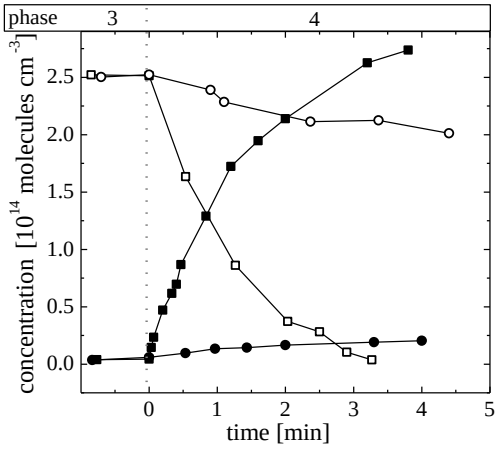

Figure 7. Photo-catalytic decomposition (i) of CO (○) and formation of CO_2 (●) in phases 3 and 4 after an Ar plasma pre-treatment in phase 1 and (ii) decomposition of CO (▫) and formation of CO_2 (■) after an O_2 plasma pre-treatment in phase 1 (Ar RF plasma: p = 0.26 mbar, ϕ = 14 sccm, t = 40 min, O_2 RF plasma: p = 0.53 mbar, ϕ = 14 sccm, t = 30 min, initial gas mixture: 1% CO in Ar, p = 1.3 mbar, UV light exposure in phase 4) [51], © IOP Publishing. Reproduced with permission. All rights reserved.

This experiment shows, that (i) O_{ads} are not reactive towards CO although they are reactive towards C_2H_2, i.e., the reactivity is dependent on the both the surface material and the target molecule, (ii) that the O atoms of the TiO_2 material are not very effective for photo catalytic oxidation of CO, and (iii) O_{ads} can be effectively used in photo catalytic oxidation [88].

2.3.2. Surface Vibrational Relaxation of N_2 Studied by Titration

Time resolved QCLAS with three pulsed lasers combined with numerical simulation has been used successfully to study the surface relaxation of N_2 by titration with CO, CO_2 and N_2O [46,52]. Vibrationally excited N_2 plays an important role in plasma chemistry, gas lasers and atmospheric re-entry. In nitrogen containing plasmas, vibrationally excited $N_2(v)$ acts as an energy reservoir that affects the electron kinetics, chemistry and thermodynamic properties of the plasma. In the case of gas discharges in mixtures containing nitrogen, electron impact vibrational excitation of N_2 often dominates the electron energy balance. Vibrational-translational/rotational (V-T/R) relaxation in N_2 is very slow. Therefore, high degrees of vibrational excitation of N_2 may be reached under typical discharge conditions. In bounded laboratory plasmas, relaxation on the reactor walls is the most efficient $N_2(v)$ loss mechanism at pressures up to a few tens of mbars. Therefore, knowledge of the heterogeneous deactivation probability of N_2 is crucial for plasma modeling (see [46,52] and references therein).

For gaining insight into the surface vibrational relaxation of N_2 a single plasma pulse experiment was performed that allowed control of the state of the target surface. A short, few ms long dc discharge pulse was applied to a mixture containing 0.05%–0.5% of CO, CO_2 or N_2O in N_2 at a pressure of 133 Pa. The experimental set-up consisting of the discharge tube and a three laser QCLAS spectrometer is shown in Figure 8.

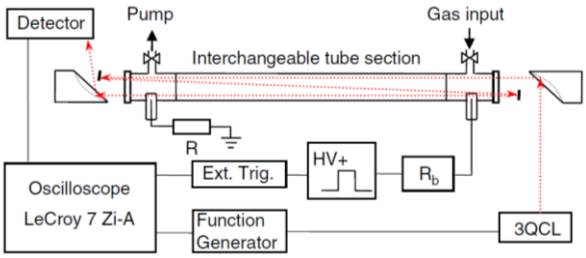

Figure 8. Experimental set-up used to study surface vibrational relaxation of N_2 [52], © IOP Publishing. Reproduced with permission. All rights reserved.

Due to the nearly resonant fast vibrational energy transfer between $N_2(v)$ and the ν_3 mode of CO_2 and N_2O and the ν_1 mode of CO_2 the vibrational excitation of the titrating molecules is a direct measure of the degree of vibrational excitation of N_2. The time evolution of the absorption signals of CO_2 and N_2O measured simultaneously in a pulsed dc discharge is shown in Figure 9.

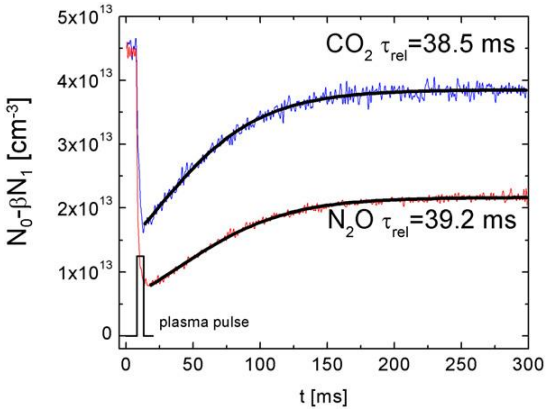

Figure 9. Time evolution of the absorption signals of CO_2 and N_2O measured simultaneously in a pulsed dc discharge at p = 133 Pa, I = 50 mA, τ = 5 ms. A fit of the experimental data is also shown. [52], © IOP Publishing. Reproduced with permission. All rights reserved.

The relaxation curves in Figure 9 were fitted to obtain a set of relaxation times τ_{rel}. The characteristic relaxation frequency $(1/\tau_{rel})$ is plotted as a function of the number density of IR tracers left after the end of the discharge pulse in Figure 10. One can see that the value of $(1/\tau_{rel})$ increases with increasing concentration of admixtures. It was demonstrated in reference [45] that the addition of CO_2 in N_2 causes a faster relaxation of $N_2(v)$ in the gas phase but also increases the probability of $N_2(v)$ quenching on the surface. The same effects may be responsible for the observed increase of $(1/\tau_{rel})$ upon the addition of CO and N_2O.

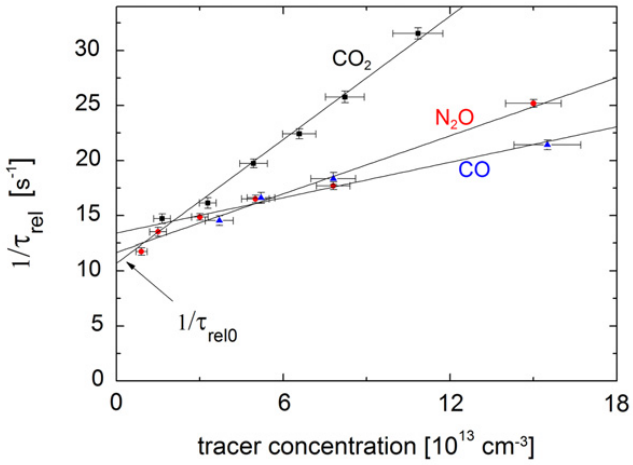

Figure 10. Characteristic relaxation frequencies $(1/\tau_{rel})$ as a function of the concentration of IR tracers left after the discharge pulse. The solid lines show a linear fit of the experimental data [52],

The effective relaxation probability and the degree of vibrational excitation of N_2 were determined in situ from the time resolved absorption measurements of CO, CO_2 and N_2O in the afterglow of the discharge at short duration. Under the low pressure conditions in this study, the main loss mechanism of vibrationally excited N_2 was wall deactivation.

The deactivation probability, γ_{N2}, was found from the best fit between the measured and simulated relaxation kinetics of CO, CO_2 and N_2O. In the model, used in this study, it was assumed that γ_{N2} for different vibrational levels of N_2 is proportional to the vibrational quantum number $\gamma_{N2}(v) = \gamma_1 \cdot v$. It was found that on Pyrex and fused silica surfaces $\gamma_1 = (1.1 \pm 0.15) \times 10^{-3}$.The quenching probability on the TiO_2 surface was measured to be $\gamma_1 = (9 \pm 2) \times 10^{-3}$ and $\gamma_1 \geqslant 4 \times 10^{-2}$ for smooth and TiO_2 particle impregnated sol-gel films, respectively.

The effect of a plasma exposure of silica on the probability of the surface vibrational relaxation of $N_2(v)$ was investigated in more detail. For this purpose, first the discharge tube was pretreated by a flowing rf discharge in N_2, O_2 or Ar for 30 min at a pressure p = 53 Pa. Then in N_2O in N_2 (or CO_2 or CO), single dc pulse experiments were performed with different admixture concentrations in the range of 0.05%–0.5% to the N_2 feed gas.

The effective relaxation frequency $1/\tau_{rel}$ in the silica reactor pretreated by N_2 or O_2 or Ar plasma as a function of the concentration of the IR tracer N_2O is shown in Figure 11. The data points were fitted with first order polynomials in order to obtain the effective relaxation frequency at a zero admixture $1/\tau_{rel0}$. From these experimental results it can be concluded that depending on the pretreatment by low-pressure plasmas (N_2 or Ar or O_2), the value of γ_1 may be changed by a factor of about 2. A detailed analysis of the relaxation kinetics of $N_2(v)$ measured with different tracers revealed new pathways for the vibrational energy accommodation on the surface. It was found that adsorbed atoms and molecules may significantly alter the probability of vibrational relaxation on a silica surface.

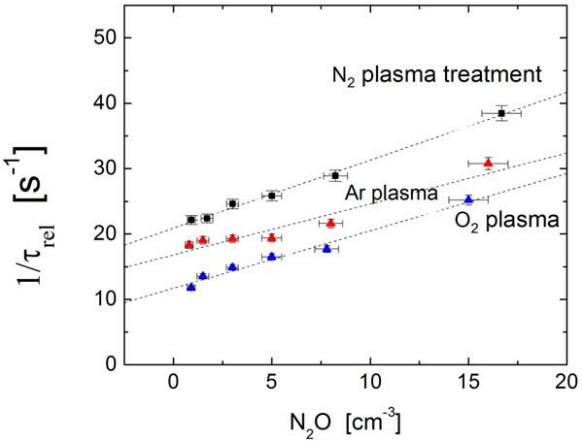

Figure 11. Effective relaxation frequency $1/\tau_{rel}$ in a silica reactor, pretreated with a N_2, O_2 or argon plasma, as a function of the concentration of the IR tracer N_2O [52], © IOP Publishing. Reproduced with permission. All rights reserved.

This study showed that IR titration coupled with QCLAS is a reliable technique for the determination of the quenching probability of vibrationally excited nitrogen molecules on a wide range of materials relevant to plasma technology.

2.4. Kinetic Studies of NO Formation in Pulsed Air-Like Low-Pressure dc Plasmas

The physics and chemistry of plasmas containing nitrogen and oxygen as main components have been the focus of a wealth of experimental and theoretical studies for fundamental and applied research in the past decade. Air-like plasmas, either at atmospheric or lower pressures, are used in various fields, including air depollution, decontamination, surface treatment and film deposition. NO is one of the main molecular components that is produced in air-like plasmas under low pressure or atmospheric conditions. NO is often considered an undesirable toxic by-product but it has also been used for the determination of gas temperature, as a source for UV radiation, or to study aspects of plasma surface interactions. Therefore, the production and decomposition of NO in its ground and excited states has been extensively investigated experimentally, see reference [6] and references therein.

The kinetics of the formation of NO in pulsed air-like dc plasmas at a pressure of 1.33 mbar and mean currents between 50 and 150 mA with 5 ms discharge pulses has been investigated both experimentally and by self-consistent numerical modelling. Using time resolved quantum cascade laser absorption spectroscopy, the densities of NO, NO_2 and N_2O have been measured in synthetic air as well as in air with 0.8% of NO_2 or N_2O. Figure 12 shows a schematic sketch of the experimental set-up consisting of a closed tube reactor made of Pyrex and a 3 channel QCLAS spectrometer, TRIPLE Q [15].

The time-dependent model used comprises a time-dependent Boltzmann equation for the electrons, a system of rate equations for the various heavy particles, and the current balance equation for the determination of the time-dependent electric field. The plasma-chemistry model distinguishes 95 species. Besides the electrons, various molecular and atomic species have been taken into account. The molecular nitrogen is assumed to be redistributed over 46 vibrational levels of the electronic ground state as well as the seven electronically excited states. As an example, Figure 13 shows the temporal evolution of selected atomic species and of electronically excited nitrogen molecules in the case of a current of 150 mA [64].

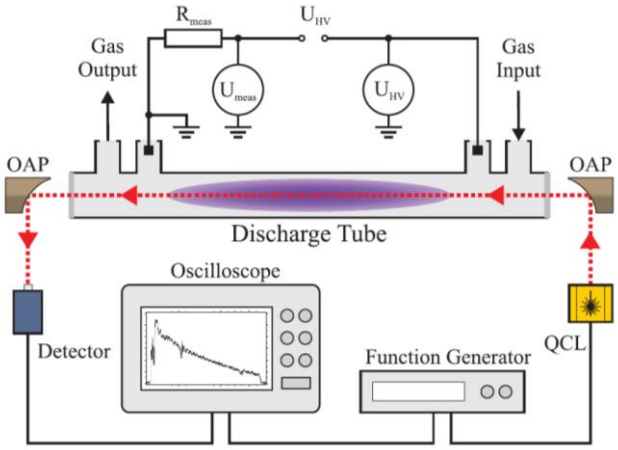

Figure 12. Experimental set-up. OAP: off-axis parabolic mirror; QCL: quantum cascade laser; R_{meas} = 18.4 Ω; U_{HV}: HV pulse generator; U_{meas}: HV probe for voltage measurement. The electrodes are represented by the two black rods inside the T-shaped holder [64], © IOP Publishing. Reproduced with permission. All rights reserved.

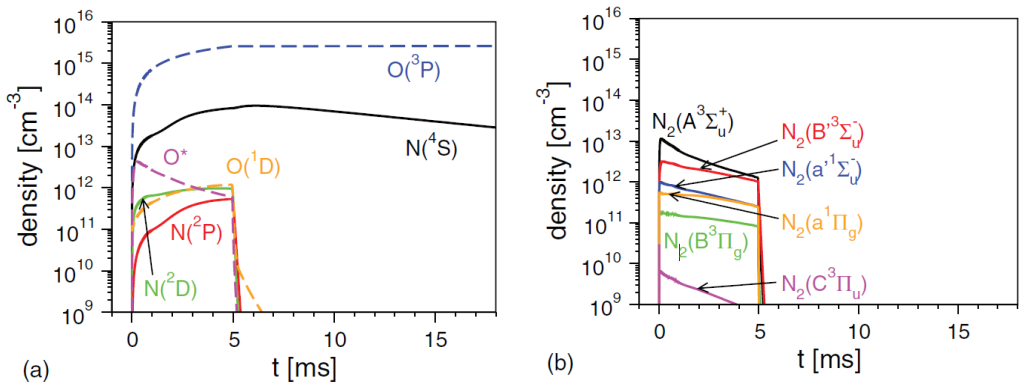

Figure 13. (**a**) Temporal evolution of selected atomic species and (**b**) of electronically excited nitrogen molecules for the case of a current of 150 mA [64], © IOP Publishing. Reproduced with permission. All rights reserved.

The temporal evolution of the NO density, presented in Figure 14, shows four distinct phases during the plasma pulse and the early afterglow in the three gas mixtures that were used. In particular, a steep density increase during the ignition phase and after termination of the discharge current pulse were detected. During phase I the discharge ignites, where there is a steep rise of the discharge current, accompanied by a strong growth of the NO density. At the same time the gas temperature increases from about 300 to 500 K. When the current reaches its maximum value, the rate of NO production diminishes slightly and the increase of the NO density is slower (active phase—phase II), while the gas temperature remains almost constant.

After the current pulse terminates, the early afterglow phase begins (phase III). Here, the density of NO continues to increase again, and with a slightly increased rate compared to phase II. The enhancement of the NO density terminates about 2 ms after the end of the active phase. During the late afterglow (phase IV) the measured NO density remains nearly unchanged and the gas temperature approaches to the ambient temperature. As is clear from Figure 14, the experimental temporal behavior is reproduced quite well by the model calculation during phases I to II. However, the calculated NO density exhibits only a slight increase during phase III rather than the measured increase of about 50%. Furthermore, the model fails to describe the almost constant NO density measured during phase IV and instead predicts a decrease of the NO density, similar to the modelling studies reported in [90].

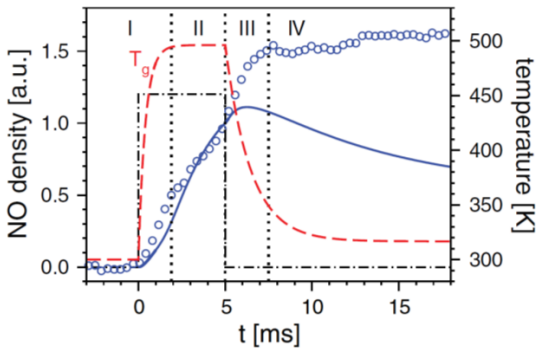

Figure 14. Temporal evolution of the measured (symbols) and calculated (full line) NO density in synthetic air for I = 150 mA. The dashed line represents the gas temperature. The dashed-dotted line is the plasma pulse [64], © IOP Publishing. Reproduced with permission. All rights reserved.

The NO concentration was found to reach a constant value of 0.57 × 10^{14} molecules cm^{-3}, 1.05 × 10^{14} molecules cm^{-3}, and 1.3 × 10^{14} molecules cm^{-3} for mean plasma currents of 50 mA, 100 mA and 150 mA, respectively. The measured densities of NO_2 and N_2O in the respective mixture decrease exponentially during the plasma pulse and remain almost constant in the afterglow, especially where the admixture of NO_2 has a remarkable impact on the NO production during the ignition. The numerical results of the coupled solution of a set of rate equations for the various heavy particles and the time-dependent Boltzmann equation of the electrons agree quite well with the experimental findings for the different air-like plasmas. The main reaction processes have been analyzed on the basis of the model calculations.

2.5. Industrial Process Monitoring in Low-Pressure Plasmas

Plasma-based etching technology has been of key importance in the semiconductor industry for several decades. The ongoing enhancement of integrated circuit performance is still governed by Moore's law. So far, the focus has been on shrinking the feature size in order to maximize the transistor density. To further improve performance, the next step is a further reduction of parasitic interlevel and intralevel capacitances by using low-k dielectrics, i.e., using a material with a lower dielectric constant than silicon dioxide. Nowadays, this is achieved by using of porous SiCOH, which is an ultra low-k material with a dielectric constant less than 2.5 [59]. The low-k material SiCOH has been of special interest, e.g., in the field of inter-level dielectrics see [58] and references therein.

In a recent study, low-pressure rf plasmas have been applied for etching of ultra-low-k SiCOH wafers using an Oxford Plasmalab System 100 (Oxford Plasma Technology, Bristol, UK). Figure 15 shows the experimental arrangement of the inductively coupled plasma (ICP) reactor, Oxford Plasmalab system 100, combined with a Q-MACS Process fiber system containing two pulsed QCLs. Multi-pass optics was implemented to achieve an absorption length of up to 8 m. The gaseous reaction products were detected in the region above the wafer. In pure CF_4 plasmas, SiCOH layers have been etched for different power values. The correlation of online and in situ measured concentrations of two etching products, CO and SiF_4, with the etching rates determined ex situ has been studied using quantum cascade laser absorption spectroscopy in the mid infrared spectral range.

In order to evaluate the influence of a standard O_2 cleaning procedure on the conditioning of the plasma reactor, experiments have been performed with or without O_2 plasma pretreatment. The results for the time dependent CO concentration are given in Figure 16. Without an O_2 plasma pretreatment no strong maximum of the CO concentration was observed at the beginning of the experiment.

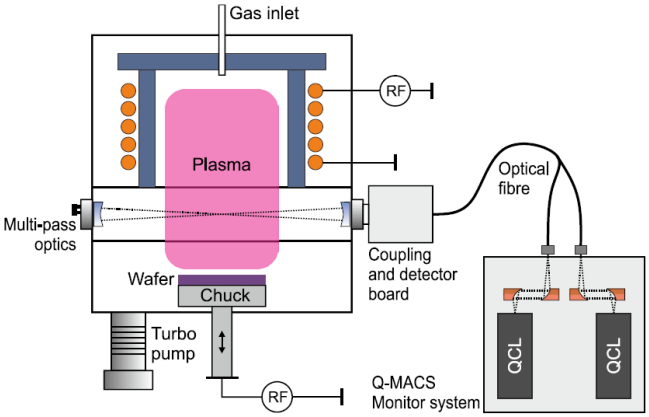

Figure 15. Experimental arrangement of the inductively coupled plasma (ICP) reactor, Oxford Plasmalab system 100, combined with a Q-MACS Process fiber system containing two pulsed QCLs [58], © Springer Publishing. Reproduced with permission. All rights reserved.

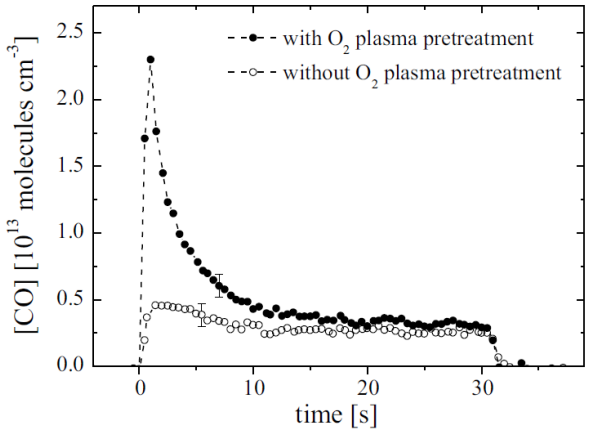

Figure 16. Time dependent CO concentration with and without O_2 plasma pretreatment (CF_4 plasma, ϕ = 12 sccm, p = 1.6 Pa). (Pretreatment: t = 3 min, p = 1.3 Pa, P = 1.5 kW, ϕ_{O2} = 30 sccm) [58], © Springer Publishing. Reproduced with permission. All rights reserved.

The concentration of SiF_4 was found to range between 0.6 and 1.4 $\times$ 10^{13} molecules cm^{-3}. In contrast the concentrations of CO were measured to be only about 50% of the SiF_4 density with a maximum of 7 $\times$ 10^{12} molecules cm^{-3}. The production rate of SiF_4, determined from the time behavior of its concentration after plasma ignition, was found to be between 1 and 5 $\times$ 10^{12} cm$^{-3}\cdot$ s^{-1}. The etching rates varied between 2 and 7 nm$\cdot$ s^{-1}. Both parameters increase nearly linearly with the applied rf power. It was found that for power values of up to 1.1 kW, the etching rate depends nearly linearly on the concentrations of both etching products monitored in situ. The etching rate (ER) of the SiCOH material can be described by its dependence on the stationary concentration of SiF_4 as:

$$ER_{SiCOH}\,(\text{nm}\cdot\text{s}^{-1}) \;=\; 4.64\times10^{13}\,[SiF_4] - 1.18 \qquad (1)$$

where [SiF_4] is given in units of 10^{13} molecules cm^{-3}, see Figure 17. Therefore, the concentration of the etching products can be directly used as a measure of the etching rate. The QCLAS approach, chosen in the present study, has proved the feasibility of a new technologically relevant in situ monitoring method for the direct online control of etching processes.

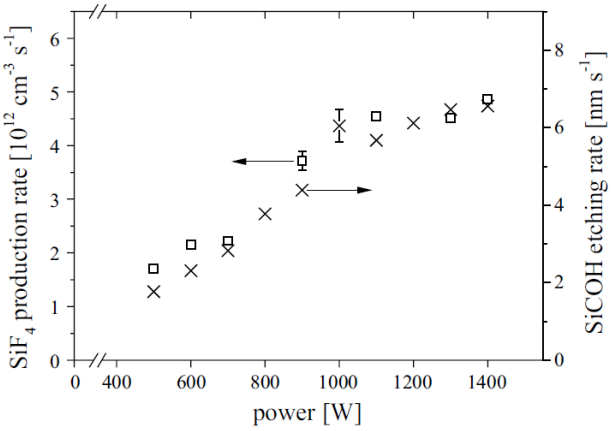

Figure 17. Production rate of SiF_4 and the etching rate of SiCOH dependence on power (CF_4 plasma, ϕ = 12 sccm, p = 0.93 Pa) [58], © Springer Publishing. Reproduced with permission. All rights reserved.

2.6. Plasma Chemistry Studies in Atmospheric Pressure Plasma Jets

2.6.1. On the Production of NO and N_2O in a Microscale Atmospheric Pressure Plasma Jet

The cold atmospheric pressure radio frequency (RF) plasma jet is considered to be a promising technology in a wide range of biological and medical applications. The underlying chemistry, however, is complex and requires characterization on multiple levels to ensure an efficient and a safe treatment [54,56,61].

Recently, absolute densities of nitrous species were monitored in a microscale atmospheric pressure RF plasma jet (μ-APPJ). The measurement of NO and N_2O densities was performed mainly by means of ex situ QCLAS via a multi-pass cell in Herriot configuration. Figures 18 and 19 show the set-up of the μ-APPJ with adjacent absorption cell. The infrared laser beam from a QCL and a collinear beam from a removable alignment laser undergo N = 38 passes through the cell which is filled with the exhaust from the plasma jet.

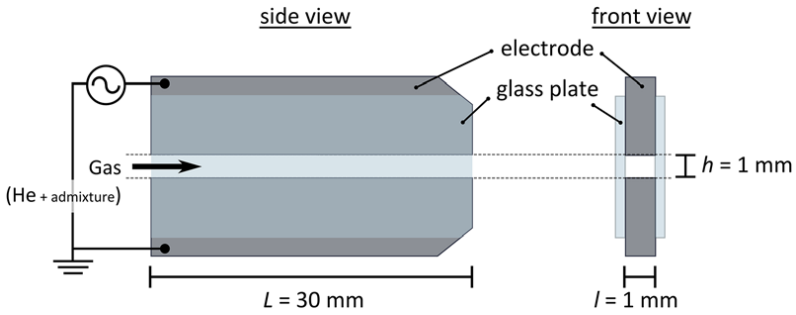

Figure 18. Schematics of a microscale atmospheric pressure RF plasma jet (μ-APPJ) source [65], © IOP Publishing. Reproduced with permission. All rights reserved.

The dependence of species production on individual parameters such as power, flow and oxygen, nitrogen and water admixture were the primary interests. NO and N_2O densities were found to increase with absorbed power, while an increase in the gas flow induced a decrease of these densities due to a reduction in residence time of the gas in the plasma. Actually, a change of these two parameters, absorbed power and gas flow, induced a variation of energy density. The higher the energy density selected the higher the NO and N_2O densities that was measured. The NO and N_2O densities were strongly gas mixture dependent. Figure 20 shows the absolute concentrations of NO and N_2O produced by the micro plasma jet as a function of the absorbed power for a helium flow of 1.4 slm with constant

1400 ppm O_2 and 7100 ppm N_2 admixture. NO and N_2O densities increased as a function of the absorbed power, which confirms the results of previous studies [10,91].

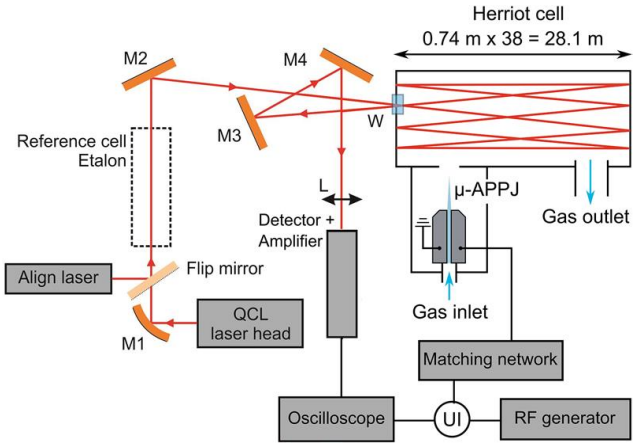

Figure 19. Set-up of the μ-APPJ with adjacent absorption cell [65], © IOP Publishing. Reproduced with permission. All rights reserved.

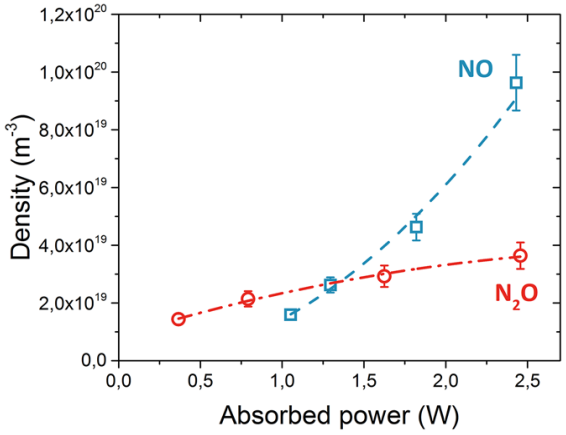

Figure 20. Absolute concentration of NO **(blue** square) and N_2O (**red** circle) produced by the micro plasma jet as a function of the absorbed power for a helium flow of 1.4 slm with constant 1400 ppm O_2 and 7100 ppm N_2 admixture. The dashed blue line and the dashed dot red line are the polynomial fit of NO and N_2O densities, respectively [65], © IOP Publishing. Reproduced with permission. All rights reserved.

A change of these parameters allows us to choose between a NO-rich or a N_2O-rich regime. NO and N_2O densities increase as a function of the N_2 admixture, while increasing oxygen, above a minimum value, reduces the densities of both NO and N_2O. When adding water instead of oxygen to the gas mixture the reduction in the NO density is much less. For maximal NO and N_2O formation a ratio of about $He/N_2/O_2 = 99.5/0.36/0.07$ is found to be the most efficient in the μ-APPJ. However, it was noted that the absorbed power in the plasma always reduced with increasing admixtures. The results obtained with QCLAS have been validated using mass spectrometry showing how the two measurement techniques can complement each other [65]. A comparison of absolute densities of nitrous species from the μ-APPJ obtained by molecular beam mass spectrometry (MBMS) and IR absorption for different spatial positions for a ratio of $He/N_2/O_2 = 99.58/0.35/0.07$ at 1.4 slm gas flow is shown in Figure 21. Note the much smaller error bars of the IR absorption data. The trend agrees

very well; the densities of all species decrease monotonically downstream from the jet, while more reactive compounds such as N decays faster than, e.g., NO.

The comparison shows that IR and MBMS can be used for mutual validation and provide a valuable addition to each other; the high spatial resolution of MBMS versus the high accuracy of IR absorption in a multi-pass cell configuration. Moreover, not only the densities in close proximity of the plasma jet for direct treatment, but also in the far field of the effluent for indirect treatment or to determine if safety limits were monitored [65].

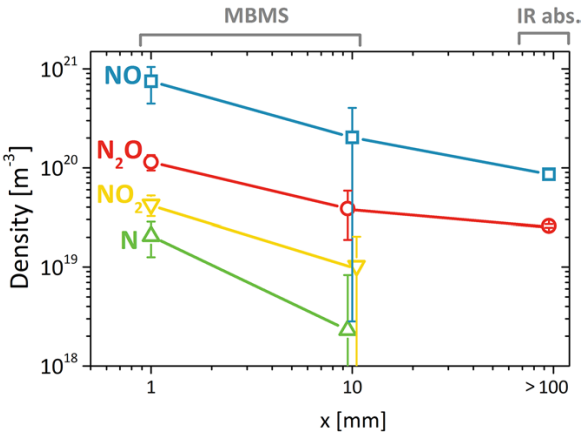

Figure 21. Comparison of absolute densities of nitrous species from the μ-APPJ obtained by molecular beam mass spectrometry (MBMS) (for x = 1 and 10 mm) and IR absorption (>100 mm) for a ratio of $He/N_2/O_2$ = 99.58/0.35/0.07 at 1.4 slm gas flow. The connecting lines are to show the reader the different decay constants of the species [65], © IOP Publishing. Reproduced with permission. All rights reserved.

2.6.2. On the Dynamics of the NO_2 Production of an Ar/Air Plasma Jet

Recently, QCLAS was used for determining the NO_2 production rate from a plasma jet operating under ambient conditions and pressure. A special type of rf argon plasma jet, kinpen, was investigated and placed in a multi-pass cell with open gas flux [54].

Figure 22 shows the experimental set-up based on a QCL diagnostic absorption system in combination with the plasma jet. The system contains various reflection optics such as planar mirror (PlM), off axis parabolic mirror (here PaM is used as abbreviation), spherical mirror (SM), and a red laser diode for optical alignment of the IR beam. The plasma jet was inserted through the glass chamber wall in such a way that the plasma effluent, a few mm long, is exhausted into the chamber. The so-called far field is defined as post-effluent, where short lived plasma species are not relevant, and considered here as the volume of the chamber (3.6 L). An algorithm for the measurements, was developed to perform a fit of the background radiation. Due to pressure broadening, the observed transitions, in this case NO_2, are broadened so much that the zero values absorption cannot be observed directly with the laser system. By performing a background measurement and by including a fitted polynomial of this background into the fit of the absorption signal, with data taken from a spectral database, the absolute densities of NO_2 was obtained. The accuracy of the measurements was determined to be down to 20 parts per billion (pbb) for both NO and NO_2 molecules. As an example, the transmittance spectrum of NO_2 produced in the jet at atmospheric pressure is plotted in Figure 23 [54].

The technique described above was used to investigate the far-field NO_2 production dynamics as a function of dry air admixture to the plasma jets feed gas. A non-linear increase was observed at small admixtures whereas a linear increase took place for levels up to 0.3% of admixed air. Figure 24 presents the net production rate of NO_2 in the far field of the argon plasma jet as a function of air admixture to the feed gas. The NO_2 generation increases strictly monotonically and does not seem to reach a local maximum until 2.0% admixture of air.

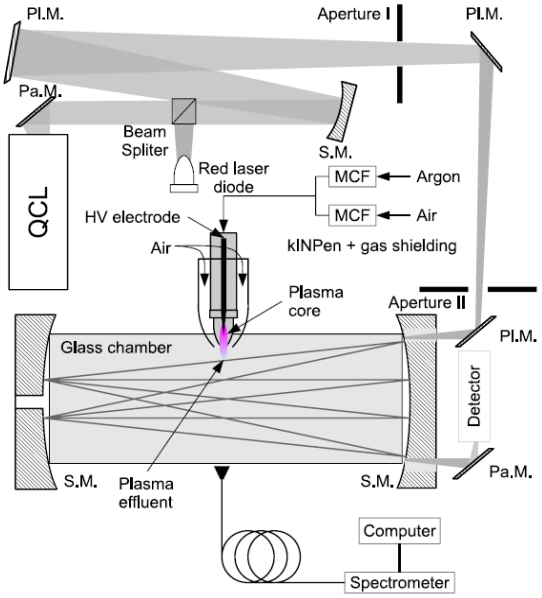

Figure 22. Schematic diagram of the spectroscopic experimental set-up based on a QCL absorption diagnostic system implementing the plasma jet. [54], © IOP Publishing. Reproduced with permission. All rights reserved.

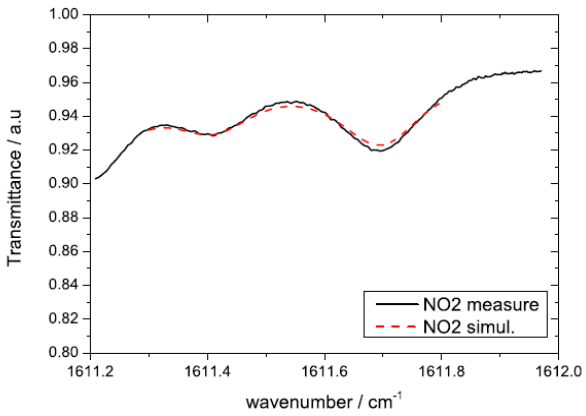

Figure 23. Transmittance spectrum of NO_2 produced by the jet at atmospheric pressure combined with a real-time fit [54], © IOP Publishing. Reproduced with permission. All rights reserved.

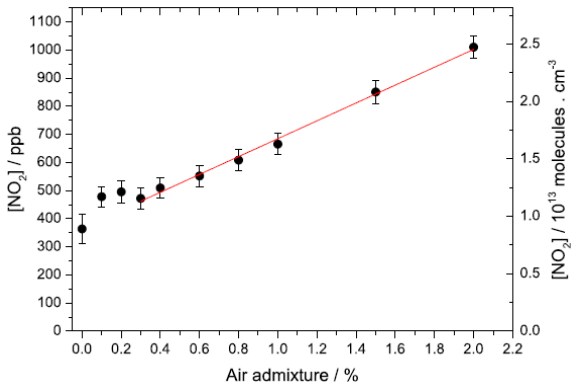

Figure 24. Absolute concentration of NO_2 produced by the kinpen for different dry air admixtures [54], © IOP Publishing. Reproduced with permission. All rights reserved.

The NO dynamics were also investigated from spectroscopic emission measurements. The NO density correlates with the NO emission for low admixtures of dry air. These measurements were performed because, with QCLAS, NO could not be detected within the multi-pass cell for the plasma jet investigated, which mainly produces oxygen containing species. The NO emission dynamic at air admixtures below 0.2% exhibits a non-linear increase, while at admixtures of greater than 0.4% this becomes an increasingly linear increase, which supports the interpretation that dissociation of N_2 and O_2 at low admixtures dominates the NO and NO_2 dynamic. The study yields a new way to investigate NO_2 production mechanisms in a plasma jet at atmospheric conditions that is almost identical to that used in applications such as plasma medicine. Far-field measurements such as the ones described in this study can be used to investigate the reactive species production processes under varying parameters and will help us to understand and control the reactive species component composition to tailor, e.g., biological responses to plasma treatment in plasma medicine.

3. Application of Continuous Wave QCLs

Within the last few years, DFB-cw-QCLs have become increasingly available and possess the advantages of pulsed lasers, namely near room temperature operation and continuously tuneable single mode emission. DFB-cw-QCLs are characterized by convenient tuning options comparable to the older TDLAS. The application of cw QCLsenables higher signal to noise ratios to be achieved due to the higher output power levels of QCLs compared with TDLs. Additionally, intensity fluctuations, which are inherent in pulsed QCLs, are considerably reduced.

3.1. On Practical Silicon Deposition Rules Derived from Silane Monitoring

Silane (SiH_4) is a process gas that is widely used throughout the semiconductor industry, especially in the production of solar modules and thin film displays. The active silicon layers of such devices are typically deposited in plasma-enhanced chemical vapor deposition (PECVD) systems. While the input SiH_4 flow rate is quantitatively controlled, SiH_4 is hardly ever monitored in the reactor itself or in the pumping line of PECVD systems. The purpose of this study was to show the relevance of monitoring physical quantities such as the SiH_4 consumption efficiency, the SiH_4 concentration in the plasma itself, or the time evolution of the SiH_4 density after ignition, to name a few.

In a recent study, the SiH_4 consumption efficiency, g, and the depletion fraction, D, were measured by monitoring silane in the pumping line and the reactor of a PECVD system, respectively. Figure 25 shows the experimental arrangement of the QCLAS spectrometer and the PECVD system [57]. Although they are closely related to one another, g and D represent two distinct physical quantities. While g is the SiH_4 consumption efficiency of the overall PECVD system, D is position-dependent and expresses the fraction by which the SiH_4 density decreases upon ignition of a discharge. Under uniform deposition conditions and in the absence of polysilane or powder formation, g is proportional to the deposition rate. Above a certain powder formation threshold, any additional amount of SiH_4 consumed was found to translate into increased powder formation rather than into a faster growing Si film. The phase of the growing Si film is correlated to the silane concentration in the plasma. On a non-crystalline substrate (glass, a-Si:H, μc-Si:H), microcrystalline Si and amorphous Si grow systematically below and above a threshold value, respectively. Within the transition region, situated between 1% and 2.8% for thin films deposited at 453 K, it is not possible to predict the phase of the growing Si film. Similarly, on a c-Si substrate, Si epitaxy and a-Si:H grow systematically below and above a threshold value [57].

The time-resolved SiH_4 density was also acquired throughout the termination of a plasma, as illustrated in Figure 26 for two sets of process conditions (A and B). The plasma was simply terminated by switching off the RF power. The gas residence time of processes A and B was 442 ms and 1.87 s, respectively. The latter is similar to the respective transition times required to reach steady state conditions upon termination of the plasma.

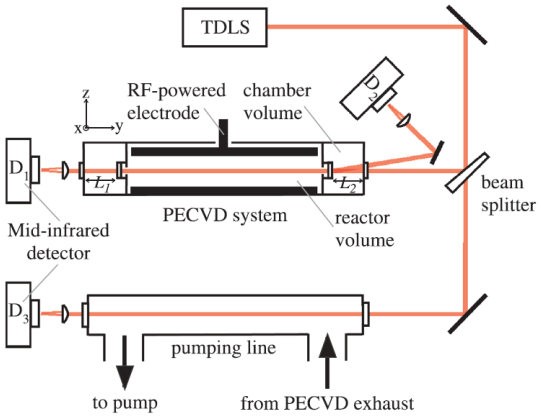

Figure 25. Experimental arrangement of the tunable diode lasers (TDLs), using a cw QCL, and the plasma-enhanced chemical vapor deposition (PECVD) system. Silane is monitored in the reactor volume (D_1), in the chamber volume (D_2), and in the pumping line (D_3) of the PECVD system [57], Reproduced from [57], with the permission of AIP Publishing.

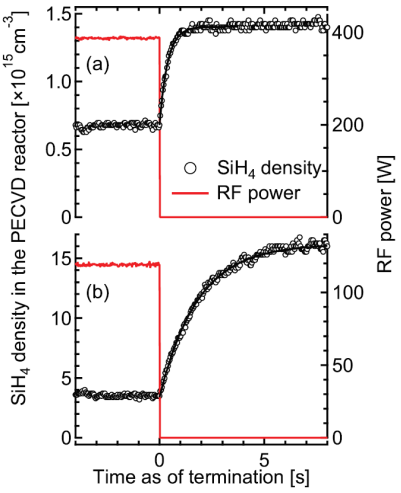

Figure 26. Plasma termination in a PECVD reactor for process A (**a**) and process B (**b**). In process A, Q_{SiH4}; Q_{H2}, and p were 45 sccm, 1980 sccm, and 4 mbars, respectively. In process B, a pressure of 1 mbar was maintained in the reactor with a pure input SiH_4 flow rate of 120 sccm. Upon termination of the plasma, the SiH_4 recovers its undepleted value with a time constant of 390 ms (**a**) and 1.82 s (**b**) (as obtained from an exponential fitting procedure). The time constant is similar to the gas residence time of the respective process [57], Reproduced from [57], with the permission of AIP Publishing.

3.2. Monitoring of CF_2 Concentrations as a Diagnostic Tool for Dielectric Etching Plasma Processes

Dielectric etching plasma processes for modern interlevel dielectrics become more and more complex with the introduction of new ultra low-k dielectrics. One challenge is the minimization of sidewall damage, where etching ultra low-k porous SiCOH using fluorocarbon plasmas. The optimization of this process requires a better quantification of the concentration of the CF_2 radical, which acts as a precursor in the polymerization of the etch sample surfaces.

Recently, the CF_2 radical was measured in situ in an industrial dielectric etching plasma reactor using a continuous wave quantum cascade laser (cw-QCL). Experiments were carried out in an Oxford Plasmalab System 100 inductively coupled plasma (ICP) etch chamber equipped with a QCL based absorption spectroscopy system (Q-MACS Process fiber, neoplas control GmbH) as schematically depicted in Figure 27 [59].

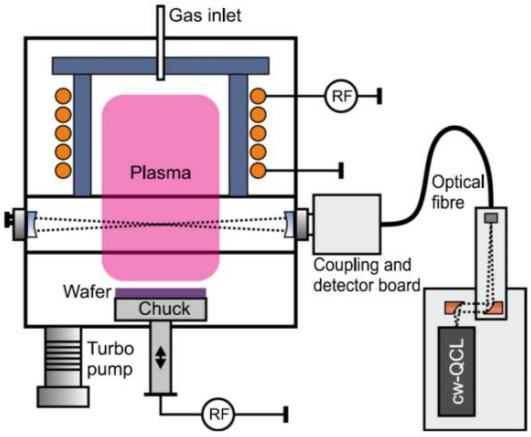

Figure 27. Outline of the Oxford Plasmalab System 100 ICP etch chamber equipped with Q-MACS Process fiber system. CF_2 radicals were detected using a multipass cell just above the wafer [59], Reproduced from [59], with the permission of AIP Publishing.

Doppler-resolved ro-vibrational absorption lines in the ν_3 fundamental band of CF_2 were monitored leading to the determination of absolute densities with the aid of an improved simulation of the line strengths. Figure 28 shows the time dependent CF_2 concentration for two characteristic cases during etching of (i) a blank porous SiCOH wafer; and (ii) of a structured porous SiCOH wafer.

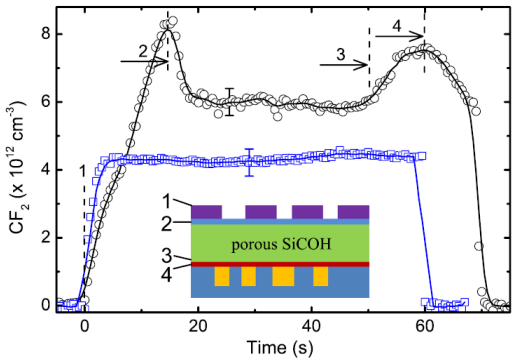

Figure 28. Time dependent CF_2 concentration while etching blank porous SiCOH (squares) and structured porous SiCOH (circles) using a CF_4 plasma with a rf power of 1000 W, bias power of 60 W, 1.33 Pa total pressure, and a gas flow rate of 25 sccm. The inset shows a schematic diagram of the lateral cross-section of a structured porous SiCOH wafer. The numbers in the upper curve represent the numbers given as the inset [59], Reproduced from [59], with the permission of AIP Publishing.

It was found that the CF_2 radical concentration during the plasma etching process directly correlated with the layer structure of the etched wafer. Hence, this correlation can serve as a diagnostic tool of the dielectric etching plasma processes. Applying QCL based absorption spectroscopy opens up the way for advanced process monitoring and etch control in semiconductor manufacturing industry.

4. Applications of External Cavity QCLs

External cavity QCLs (EC-QCLs) have high potential for applications for plasma diagnostics purposes, based on their intrinsic properties, in particular wide spectral tunability, intrinsic narrow linewidth and high output powers. These properties do not only allow the monitoring of multiple species but also of larger plasma molecules characterized by broader spectral features. It should be noted that due to the very narrow mode spacing of continuous wave mode-hop free EC-QCLs (cw MHF EC-QCLs) stable operation at short pulse length, e.g., in the ms time scale, is not feasible [92].

A reliable concentration determination requires a periodic interruption of the laser radiation, which can be performed by mechanical choppers or shutters or by acousto-optic modulators (AOM). Reflection of light back into the EC-QCL should be avoided, because it can lead to mode instabilities. At high power values of up to several hundred mW possible non-linear effects should be considered studying molecular plasmas.

4.1. Investigations of Plasma Nitriding and Nitrocarburizing Processes

The improvement of the properties of the surface of steel components has been in the center of interest of plasma based nitriding and nitrocarburising processes since several decades. Applying the traditional technique, the conventional plasma nitriding (CPN), the metallic workload acts as a cathode while a pulsed DC discharge is used for the treatment. In a variety of industrial applications CPN is a standard technology for surface modification and surface hardening. The diffusive interaction of excited atomic and molecular species with the appropriately heated surface of the metal components is considered as the basic mechanism of this technology [63].

A modification of CPN, called active screen plasma nitriding (ASPN), replaces the glow discharge region from the workload to an additionally introduced separate metallic screen, the active screen (AS), which surrounds the components to be treated. The ASPN approach is focused on the reduction of possible disadvantages of the CPN technology, which may be caused by the direct influence of the discharge energy on the surface of the workloads, including inhomogeneous temperature distributions, as well as possible hollow cathode and arcing effects. Using the ASPN technique two important parameters, (i) the temperature of the process; and (ii) the current density of the plasma are more pronounced decoupled. In addition, the active screen has a twofold task (i) the generation of a mixture of active species for the nitriding process; and (ii) the radiation of heat leading to a relative uniform temperature distribution over the parts of the workload even in the case of complicated geometries.

Although the ASPN technology has proven its industrial applicability in the last decade, the plasma chemical phenomena are far from being completely understood. A better knowledge about the fundamental mechanisms inherent in this technology could open up a wider technological potential [62].

In a recent study, the concentrations of the carbon containing precursor and of the reaction products have been monitored in a novel developed laboratory scale ASPN reactor, named PLANIMOR, using an EC-QCL providing a mode-hop free tuning range of ν = 1345–1400 cm^{-1}. The experimental arrangement of the reactor combined with QCLAS and OES spectrometers is shown in Figure 29. The linear electrode set-up of PLANIMOR allows the detection of the molecular species in the treatment zone between the active screen and the sample holder. For an increased sensitivity the QCLAS was combined with a multi-pass optics (White cell type) mounted on the diagnostic path of PLANIMOR. With up to 20 passes an effective absorption length of l = 950 cm can be realized.

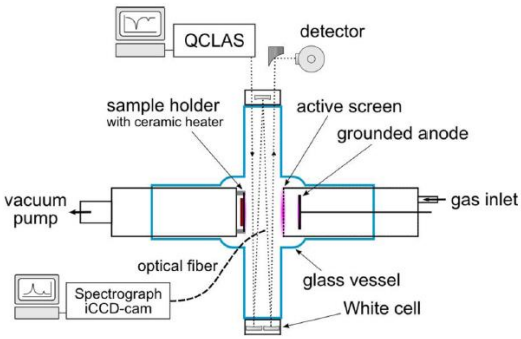

Figure 29. Experimental arrangement of the PLANIMOR model reactor combined with QCLAS and OES spectrometers. The plane of the White cell is parallel to the screen and the sample holder (it is rotated by 90° for better illustration) [63], Reproduced from [63], with the permission of AIP Publishing.

An example spectrum in the spectral range near 1356.5 cm^{-1} in the H_2-N_2 plasma with a CH_4 admixture of 2.4% at a plasma power at the active screen of P_{screen} = 90 W and a pressure of p = 3 mbar is shown in Figure 30.

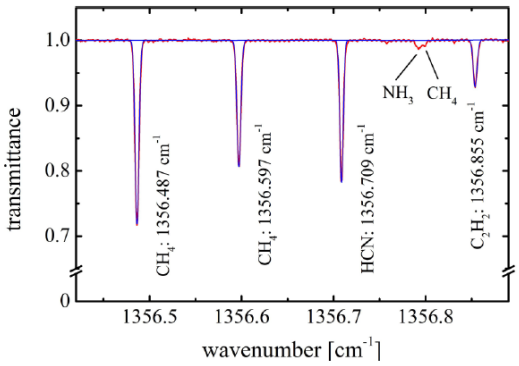

Figure 30. Example of an absorption spectrum at 1356.6 cm^{-1} with absorption features of CH_4, HCN, C_2H_2 and NH_3 (p = 3 mbar, 10 sccm H_2 + 10 sccm N_2 + 0.5 sccm CH_4, P_{screen} = 90 W) [63], Reproduced from [63], with the permission of AIP Publishing.

The ability of PLANIMOR to treat ferrous materials reaching similar nitriding results as in industrial scale ASPN reactors was shown recently [62,63]. A photograph, comparing an untreated steel (C15) sample with a sample treated in PLANIMOR (t = 4 h, P_{screen} = 90 W, T_{sample} = 823 K) using the additional plasma at the sample holder (P_{sample} = 10 W) is shown in Figure 31. A thickness of the compound layer of up to 6.2 µm was reached.

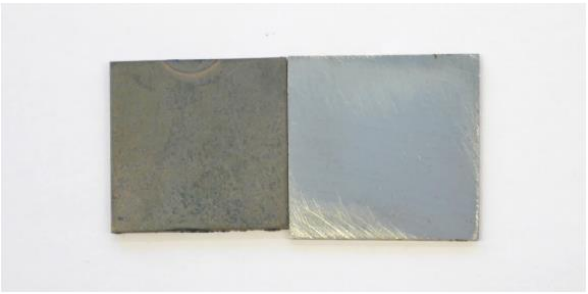

Figure 31. Comparing treated (left) and untreated (right) C15 steel samples at t = 4 h, P_{screen} = 90 W, ϕ = 20 sccm (H_2:N_2 = 1:1), p = 3 mbar, and $T_{samples}$ = 823 K [63], Reproduced from [63], with the permission of AIP Publishing.

The used QCL spectrometer allowed the detection of the precursor, CH_4, and of the reaction products NH_3, HCN and C_2H_2, while the latter had been detected the first time in situ in plasma nitrocarburizing processes due to the improved sensitivity realized with the multi-pass optics in PLANIMOR. The dependencies of the concentration of the carbon containing precursor and of the reaction products on the power of the screen plasma are shown in Figure 32. When comparing the molecular concentrations with those in a cylindrical industrial scale ASPN reactor, it was found that the plasma chemistry in both reactor types is similar [62]. Furthermore, the applied QCLAS led to deeper insights into the chemical processes of this industrial utilized technology.

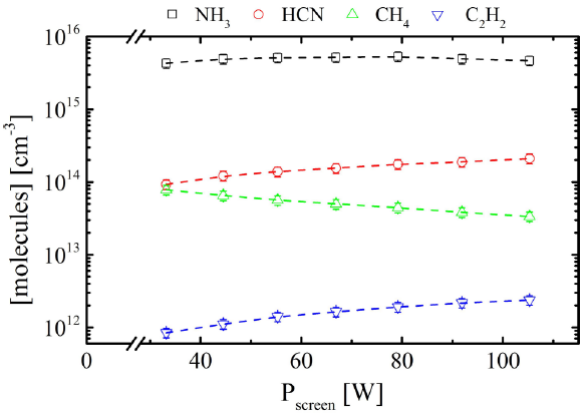

Figure 32. The concentrations of NH_3, CH_4, HCN and C_2H_2 depending on the power of the screen plasma (p = 3 mbar, 10 sccm H_2 + 10 sccm N_2 + 0.2 sccm CH_4) [63], Reproduced from [63], with the permission of AIP Publishing.

4.2. Study of Low Pressure, Low Temperature H_2-CH_4-CO_2 Microwave Plasmas Used for Large Area Deposition of Nanocrystalline Diamond Films

Nanocrystalline diamond (NCD) has many properties that are very advantageous for selected tribological and electronic applications. Although already more than two decades ago the feasibility of the deposition of nanocrystalline diamond (NCD) has been shown, the further development of this technology is still of great importance, in particular concerning the treatment of large substrates at relatively low substrate temperatures. The wider commercial use of NCD films is hampered by the requirement that the substrate temperatures have to be significantly below 800 °C in the deposition process to avoid damaging sensitive substrates. In the last few years, a new approach for the deposition of large area NCD films at relatively low substrate temperatures below 400 °C has been developed. A 4 × 4 distributed antenna array (DAA) microwave plasma reactor has successfully been employed to deposit uniform NCD films on a 4-inches wafer at substrate temperatures below 300 °C using H_2 with admixtures of few per cent of CH_4 and CO_2 as feed gas. The admixture of even a low amount of CO_2 provides additional etching species and reduces the activation energy needed for diamond growth, which allows the deposition of NCD films at very low substrate temperatures [66].

In a recent study, the physical and chemical phenomena in the complex H_2-CH_4-CO_2 microwave plasmas used for NCD deposition were investigated by a combination of optical emission spectroscopy with IRLAS in the mid infrared spectral range. The experimental arrangement of the distributed antenna array (DAA) chemical vapor deposition (CVD) reactor for depositing NCD films together with the optical diagnostics systems is shown in Figure 33 [66]. For IRLAS, a compact and mobile infrared component acquisition (IRMA) system has been utilized based on traditional tunable diode lead salt lasers as radiation sources together with an EC-QCL. Hence, the evolution of the concentration of the methyl radical, CH_3, of five stable molecules, CH_4, CO_2, CO, C_2H_2 and C_2H_6, and of vibrationally excited CO in the first and second hot band and the respective temperatures, gas, rotational, and vibrational, of all these species was monitored in the plasma processes. Information about the gas temperature and the degree of dissociation of the hydrogen molecules of the microwave plasma has been derived by the OES method [66].

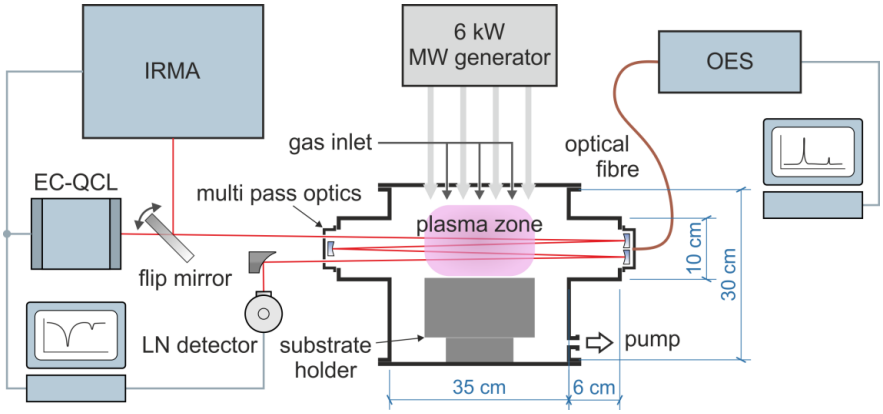

Figure 33. Experimental arrangement of the distributed antenna array (DAA) microwave reactor combined with the AS spectrometer consisting of the IRMA system and an external cavity QCL (EC-QCL) and the OES unit [66], © IOP Publishing. Reproduced with permission. All rights reserved.

Using this complex spectrometer arrangement, gas composition, rotational and vibrational temperatures were determined depending on power and pressure of the discharge, which are of great importance for calculation of species concentrations [66]. Based on this detailed temperature analysis, the concentrations of the precursor gases CH_4 and CO_2 and of the reaction products CH_3, CO, C_2H_2 and C_2H_6 were determined in a follow-up paper in which the influences of the discharge parameters power and pressure on the molecular concentrations were studied. In this way, the dissociation of the carbon precursor gases including their fragmentation and conversion to the reaction products was analyzed in detail [67].

Here, we will concentrate on the EC-QCL measurements of CO and especially show that with an EC-QCL, an extensive temperature analysis of molecules can be performed, i.e., information on the gas, rotational, and vibrational temperatures can be obtained. This EC-QCL (Daylight Solutions, MHF-21047-01, SanDiego, CA, USA) could be scanned over about 100 cm^{-1} mode hop free (2080–2180 cm^{-1}) allowing the monitoring of 44 CO lines of the ground state and of three hot bands. In Figure 34, the CO band stick spectrum containing 31 ground and hot band lines of the first excited level measured with an EC-QCL spectrometer in a H_2-CH_4-CO_2 MW plasma is presented. The small laser line width of the EC-QCL (~1×10^{-3} cm^{-1}) enabled line profile analysis with a typical uncertainty of $\pm$30 K for ground state lines. In addition, this method was applied for a variety of lines of the first, second and third hot band. Figure 35 shows experimental data of absorption lines of CO, R(1) at 2150.856 cm^{-1} of the ground state and R(17) at 2179.244 cm^{-1} of the first hot band, together with Gaussian fits for temperature determination. The lines are superposed in position and normalized in intensity in order to compare their relative broadening. It has to be considered, that the intensity ratio of lines of the ground state and the first hot band is in the range of 20 leading to different signal to noise ratios and therefore to different errors in the accuracy of the obtained temperatures. In Figure 36, the gas temperature of CO lines as a function of their rotational quantum number for the R and P branches for the ground ($\nu = 0$), the first ($\nu = 1$), second ($\nu = 2$) and third ($\nu = 3$) excited vibrational levels are presented for a pressure of 0.25 mbar. The errors of the measurement are typically in the range of 10% caused by reduced intensities causing smaller signal to noise ratios compared to ground state lines and also by influences of fluctuations mainly in the hot zones of the plasma region.

As the density of CO in a variety of quantum states in the ground and excited states was determined, it was possible to determine in how far the rotational and vibrational density distribution was characterized by a Boltzmann distribution. The rotational and vibrational temperatures were extracted from Boltzmann plots of the recorded spectra. An example is given in Figure 37 showing Boltzmann plots of the P and R branch lines of the first CO hot band for two pressure values, $p = 0.25$ and 0.35 mbar [66].

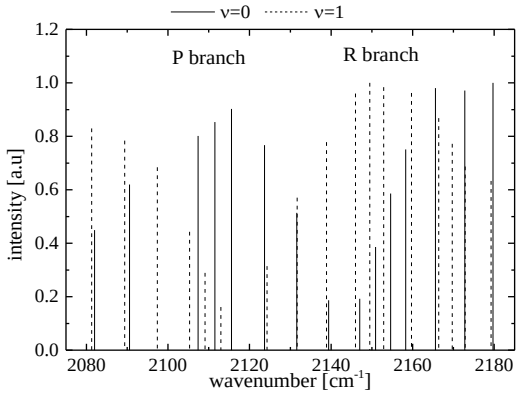

Figure 34. CO band stick spectrum containing 31 ground and hot band lines measured with an EC-QCL spectrometer. The intensities of the lines are normalized. In general, the intensities of the hot band lines are about 20 times smaller than the ground state lines, p = 0.35 mbar, P = 3 kW [66], © IOP Publishing. Reproduced with permission. All rights reserved.

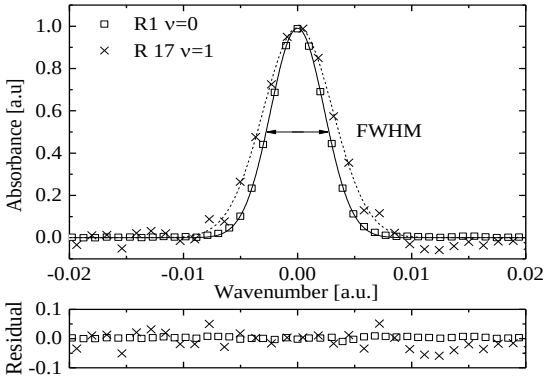

Figure 35. Experimental data of absorption lines of CO, R(1) of the ground state and R(17) of the first hot band, together with Gaussian fits for temperature determination. The lines are superposed in position and normalized in intensity in order to compare their relative broadening, p = 0.35 mbar, P = 3 kW, ϕ = 50 sccm, CH_4 admixture: 2.5%, CO_2 admixture: 1% [66], © IOP Publishing. Reproduced with permission. All rights reserved.

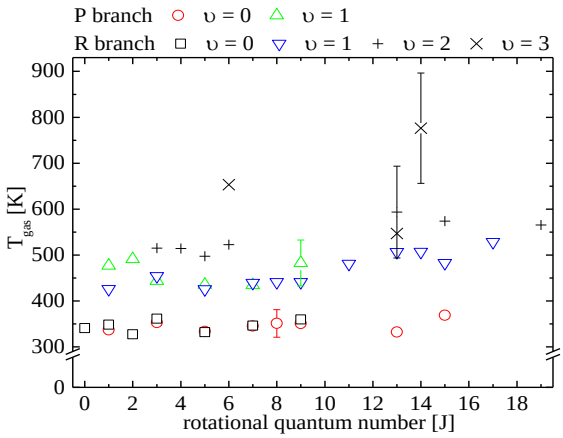

Figure 36. Gas temperature T_{gas} determined from the Doppler broadening of CO lines as a function of their rotational quantum number for the R and P branches for the ground and the first, second and third excited vibrational levels, p = 0.25 mbar, P = 3 kW, ϕ = 50 sccm, CH_4 admixture: 2.5%, CO_2 admixture: 1% [66], © IOP Publishing. Reproduced with permission. All rights reserved.

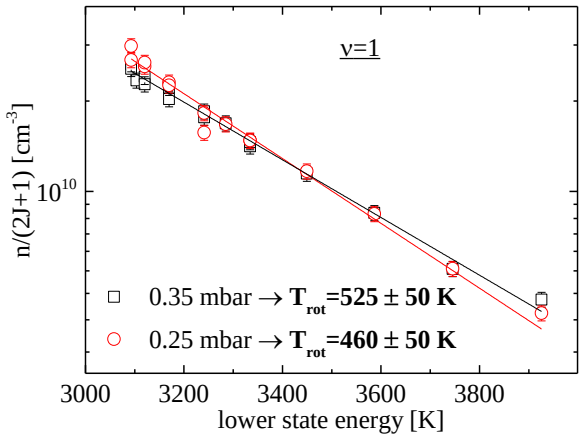

Figure 37. Boltzmann plot of the P and R branch of CO lines of the first hot band for two pressure values, p = 0.25 and 0.35 mbar, P = 3 kW, ϕ = 50 sccm, CH_4 admixture: 2.5%, CO_2 admixture: 1% [66],

It was found that the rotational temperatures in the various vibrational bands were in very good accordance to the gas temperatures derived from CO Doppler broadening analysis of lines of the ground state and of the first and second hot band of CO. The analysis of the vibrational temperatures clearly showed a non-Boltzmann distribution between the vibrational levels ν = 0 and of ν = 1−3. That ν = 0 has different population characteristics leading to a different vibrational temperature was attributed to the fact that the molecules being measured in this vibrational band were in the outer and therefore colder regions of the plasma. That T_{vib} is not equal to T_{rot}, and that T_{rot} is different for each vibrational level indicates a non-Boltzmann population distribution over the rotational-vibrational states of CO under the present plasma conditions.

In conclusion, using the EC-QCL a relatively wide spectral range with a variety of CO lines in the ground and in three excited states has been analyzed. This approach enabled an extensive temperature analysis over several vibrational levels providing new insights into energetic aspects of the multi-component non-equilibrium plasma and indicated that the plasma generation is characterized by a variety of hottest, hot and colder zones in this DAA microwave plasma reactor.

5. Summary and Conclusions

From the middle of the last decade, a variety of phenomena in molecular non-equilibrium plasmas in which many short-lived and stable species are produced have been successfully studied with quantum cascade laser absorption spectroscopy or QCLAS in the mid infrared spectral range, with which the present article is concerned. It has been possible to determine absolute concentrations of ground states using spectroscopy thereby providing a link with chemical modelling of the plasma, the ultimate objective being a better understanding of the chemical and reaction kinetic processes occurring in the plasma. The other essential component needed to reach this objective is to determine the physical parameters of the plasma, for example, temperatures, degrees of dissociation, dynamics of reaction processes and phenomena involving plasma surface interactions. The present article discusses methods for achieving these. The need for a better scientific understanding of plasma physics and chemistry has stimulated the application of QCLAS, which has proven to be one of the most versatile techniques for studying molecular plasmas. About 50 QCLAS studies in research and industry have been reported in the last few years. The papers describing these studies are compiled in Table 1. The availability of new powerful radiation sources as external cavity QCLs or recently of mid infrared frequency combs offers promising new avenues for plasma diagnostics in general and for multi-component detection in particular. Based on the recent development of advanced

instrumentation including compact and robust QCLAS systems, the spread of this method of high resolution mid infrared spectroscopy to industrial applications has rapidly materialized.

Acknowledgments: This work was partly supported by (a) the German Research Foundation (DFG) within the framework of the Collaborative Research Centre Transregio 24 "Fundamentals of Complex Plasmas"; (b) the Federal Ministry of Education and Research (BMBF), FKZ 13N7451/8 and by the Federal Ministry of Economics and Technology (BMWi), FKZ KF 0086503FK6; (c) by the EFRE fund of the European Community and by funding from the State of Saxony of the Federal Republic of Germany; (d) the German Academic Exchange Service (DAAD) and EGIDE as part of the French-German PROCOPE Collaboration Program.

The authors give sincere thanks to all present and former members of the laboratories involved in Greifswald, Palaiseau, Eindhoven and Cambridge for permanent support and a stimulating working climate. In particular, the authors are indebted to all co-authors of former papers whose contributions made the present review article possible. Finally, the authors acknowledge the support given by Neoplas Control, Alpes Lasers, Daylight Solutions and MGO Optical Solutions.

Author Contributions: J.R. and J-P.H.v.H. led the writing of the paper, with contributions from all authors.

Conflicts of Interest: The authors declare no conflict of interest.

References

1. Röpcke, J.; Lombardi, G.; Rousseau, A.; Davies, P.B. Application of mid-infrared tuneable diode laser absorption spectroscopy to plasma diagnostics: A review. *Plasma Sources Sci. Technol.* **2006**, *5*, S148–S168. [CrossRef]
2. Curl, R.F.; Capasso, F.; Gmachl, C.; Kostorev, A.A.; McManus, B.; Lewicki, R.; Pusharsky, M.; Wysocki, G.; Tittel, F.K. Quantum cascade lasers in chemical physics. *Chem. Phys. Lett.* **2010**, *487*, 1–18. [CrossRef]
3. Welzel, S.; Hempel, F.; Hübner, M.; Lang, N.; Davies, P.B.; Röpcke, J. Quantum Cascade Laser Absorption Spectroscopy as a Plasma Diagnostic Tool: An Overview. *Sensors* **2010**, *10*, 6861–6900. [CrossRef] [PubMed]
4. Lang, N.; Zimmermann, S.; Uhlig, B.; Schaller, M.; Röpcke, J.; Schulz, S.E. In situ analysis of ultra low-k etch processes using quantum cascade laser absorption spectroscopy. In Proceedings of the 30th ICPIG, Belfast, UK, 28 August–2 September 2011.
5. Guaitella, O.; Hübner, M.; Welzel, S.; Marinov, D.; Röpcke, J.; Rousseau, A. Evidence for surface oxidation on pyrex of NO into NO_2 by adsorbed O atoms. *Plasma Sources Sci. Technol.* **2010**, *19*, 045026. [CrossRef]
6. Röpcke, J.; Davies, P.B.; Lang, N.; Rousseau, A.; Welzel, S. Applications of quantum cascade lasers in plasma diagnostics: A review. *J. Phys. D Appl. Phys.* **2012**, *45*, 423001. [CrossRef]
7. Burlacov, I.; Börner, K.; Spies, H.-J.; Biermann, H.; Lopatik, D.; Zimmermann, H.; Röpcke, J. In-situ monitoring of plasma enhanced nitriding processes using infrared absorption and mass spectroscopy. *Surf. Coat. Technol.* **2012**, *206*, 3955–3960. [CrossRef]
8. Hempel, F.; Lopatik, D.; Sikimic, B.; Stefanovic, I.; Winter, J.; Röpcke, J. Monitoring of hydrocarbon concentrations in dust-producing RF plasmas. *Plasma Sources Sci. Technol.* **2012**, *21*, 055001. [CrossRef]
9. Stepanov, S.; Meichsner, J. Absolute number density and kinetic analysis of the CF radical in pulsed $CF_4 + H_2$ radio-frequency plasmas. *Plasma Sources Sci. Technol.* **2012**, *21*, 024008. [CrossRef]
10. Pipa, A.V.; Bindemann, T.; Foest, R.; Kindel, E.; Röpcke, J.; Weltmann, K.-D. Absolute production rate measurements of nitric oxide by an atmospheric pressure plasma jet (APPJ). *J. Phys. D Appl. Phys.* **2008**, *41*, 194011. [CrossRef]
11. Röpcke, J.; Mechold, L.; Käning, M.; Anders, J.; Wienhold, F.G.; Nelson, D.; Zahniser, M. IRMA: A tunable infrared multicomponent acquisition system for plasma diagnostics. *Rev. Sci. Instrum.* **2000**, *71*, 3706. [CrossRef]
12. McManus, J.B.; Nelson, D.; Zahniser, M.; Mechold, L.; Osiac, M.; Röpcke, J.; Rousseau, A. TOBI: A two-laser beam infrared system for time-resolved plasma diagnostics of infrared active compounds. *Rev. Sci. Instrum.* **2003**, *74*, 2709. [CrossRef]
13. Kazarinov, R.F.; Suris, R.A. Possibility of the amplification of electromagnetic waves in a semiconductor with a superlattice. *Sov. Phys. Semicond.* **1971**, *5*, 707.
14. Faist, J.; Capasso, F.; Sivco, D.L.; Sirtori, C.; Hutchinson, A.L.; Cho, A.Y. Quantum cascade laser. *Science* **1994**, *264*, 553–556. [CrossRef] [PubMed]

15. Hübner, M.; Welzel, S.; Marinov, D.; Guaitella, O.; Glitsch, S.; Rousseau, A.; Röpcke, J. TRIPLE Q: A three channel quantum cascade laser absorption spectrometer for fast multiple species concentration measurements. *Rev. Sci. Instrum.* **2011**, *82*, 093102. [CrossRef] [PubMed]
16. Shorter, J.H.; Nelson, D.D.; McManus, J.B.; Zahniser, M.S.; Milton, D.K. Multicomponent Breath Analysis with Infrared Absorption Using Room-Temperature Quantum Cascade Lasers. *IEEE Sens. J.* **2010**, *10*, 76–84. [CrossRef] [PubMed]
17. Hugi, A.; Maulini, R.; Faist, J. External cavity quantum cascade laser. *Semicond. Sci. Technol.* **2010**, *25*, 083001. [CrossRef]
18. Walker, R.J.; van Helden, J.H.; Richie, G.A.D. Quantum cascade laser absorption spectroscopy of the 1←0 band of deuterium bromide at 5 μm. *Chem. Phys. Lett.* **2010**, *501*, 20–24. [CrossRef]
19. Karpf, A.; Rao, G.N. Enhancement of trace gas detection by integrating wavelength modulated spectra across multiple lines. *Appl. Opt.* **2010**, *49*, 1406–1413. [CrossRef] [PubMed]
20. Furstenberg, R.; Kendziora, C.A.; Stepnowski, J.; Stepnowski, S.V.; Rake, M.; Papantonakis, M.R.; Nguyen, V.; Hubler, G.K.; McGill, R.A. Stand-off detection of trace explosives via resonant infrared photothermal imaging. *Appl. Phys. Lett.* **2008**, *93*, 224103. [CrossRef]
21. Karpf, A.; Rao, G.N. Absorption and wavelength modulation spectroscopy of NO_2 using a tunable, external cavity continuous wave quantum cascade laser. *Appl. Opt.* **2009**, *48*, 408–413. [CrossRef] [PubMed]
22. Lewicki, R.; Doty, J.H., III; Curl, R.F.; Tittel, F.K.; Wysocki, G. Ultrasensitive detection of nitric oxide at 5.33 μm by using external cavity quantum cascade laser-based Faraday rotation spectroscopy. *PNAS* **2009**, *106*, 12587–12592. [CrossRef] [PubMed]
23. Cheesman, A.; Smith, J.A.; Ashfold, M.N.R.; Langford, N.; Wright, S.; Duxbury, G. Application of a Quantum Cascade Laser for Time-Resolved, in Situ Probing of CH_4/H_2 and C_2H_2/H_2 Gas Mixtures during Microwave Plasma Enhanced Chemical Vapor Deposition of Diamond. *J. Phys. Chem. A* **2006**, *110*, 2821. [CrossRef] [PubMed]
24. Welzel, S.; Gatilova, L.; Röpcke, J.; Rousseau, A. Time-resolved study of a pulsed dc discharge using quantum cascade laser absorption spectroscopy: NO and gas temperature kinetics. *Plasma. Sources Sci. Technol.* **2007**, *16*, 822. [CrossRef]
25. Stancu, G.D.; Lang, N.; Röpcke, J.; Reinicke, M.; Steinbach, A.; Wege, S. In Situ Monitoring of Silicon Plasma Etching Using a Quantum Cascade Laser Arrangement. *Chem. Vapor. Depos.* **2007**, *13*, 351–360. [CrossRef]
26. Van Helden, J.H.; Horrocks, S.J.; Ritchie, G.A.D. Application of quantum cascade lasers in studies of low-pressure plasmas: Characterization of rapid passage effects on density and temperature measurements. *Appl. Phys. Lett.* **2008**, *92*, 081506. [CrossRef]
27. Hancock, G.; Horrocks, S.J.; Ritchie, G.A.D.; van Helden, J.H.; Walker, R.J. Time-Resolved Detection of the CF_3 Photofragment Using Chirped QCL Radiation. *J. Phys. Chem. A* **2008**, *112*, 9751. [CrossRef] [PubMed]
28. Quine, Z.R.; McNesby, K.L. Acetylene measurement in flames by chirp-based quantum cascade laser spectrometry. *Appl. Opt.* **2009**, *48*, 3075–3083. [CrossRef] [PubMed]
29. Lang, N.; Röpcke, J.; Steinbach, A.; Wege, S. Wafer2wafer etch monitor via in situ QCLAS. *IEEE Trans. Plasma Sci.* **2009**, *37*, 2335–2341. [CrossRef]
30. Ma, J.; Cheesman, A.; Ashfold, M.N.R.; Hay, K.G.; Wright, S.; Langford, N.; Duxbury, G.; Mankelevich, Y.A. Quantum cascade laser investigations of CH_4 and C_2H_2 interconversion in hydrocarbon/H2 gas mixtures during microwave plasma enhanced chemical vapor deposition of diamond. *J. Appl. Phys.* **2009**, *106*, 033305. [CrossRef]
31. Bartlome, R.; Feltrin, A.; Ballif, C. Infrared laser-based monitoring of the silane dissociation during deposition of silicon thin films. *Appl. Phys. Lett.* **2009**, *94*, 201501. [CrossRef]
32. Hempel, F.; Artyushenko, V.; Weichbrodt, F.; Röpcke, J. Application of quantum cascade lasers and infrared-fibres for the monitoring and control of industrial plasma processes. *J. Phys. Conf. Ser.* **2009**, *157*, 012003. [CrossRef]
33. Abd Allah, Z.; Sawtell, D.; Kasytich, V.L.; Martin, P.A. FTIR and QCL diagnostics of the decomposition of volatile organic compounds in an atmospheric pressure dielectric packed bed plasma reactor. *J. Phys. Conf. Ser.* **2009**, *157*, 012010. [CrossRef]
34. Welzel, S.; Stepanov, S.; Meichsner, J.; Röpcke, J. Using quantum cascade lasers with resonant optical cavities as a diagnostic tool. *J. Phys. Conf. Ser.* **2009**, *157*, 012010. [CrossRef]

35. Stepanov, S.; Welzel, S.; Röpcke, J.; Meichsner, J. Time resolved QCLAS measurements in pulsed cc-rf CF_4/H_2 plasmas. *J. Phys. Conf. Ser.* **2009**, *157*, 012008. [CrossRef]
36. Welzel, S.; Stepanov, S.; Meichsner, J.; Röpcke, J. Time resolved studies on pulsed fluorocarbon plasmas using chirped quantum cascade lasers. *J. Phys. D Appl. Phys.* **2010**, *43*, 124014. [CrossRef]
37. Lang, N.; Röpcke, J.; Wege, S.; Steinbach, A. In situ diagnostic of etch plasmas for process control using quantum cascade laser absorption spectroscopy. *Eur. Phys. J. Appl. Phys.* **2010**, *49*, 13110. [CrossRef]
38. Hempel, F.; Lang, N.; Zimmermann, H.; Strämke, S.; Röpcke, J. Plasma process monitoring of BCl^3 using high-resolution infrared laser absorption spectroscopy. *Meas. Sci. Technol.* **2010**, *21*, 085703. [CrossRef]
39. Wolter, M.; Hundt, M.; Kersten, H. Measurement of CH_4-concentration in HMDSO-containing process plasmas by quantum cascade laser absorption spectroscopy. *Vacuum* **2010**, *85*, 482–485. [CrossRef]
40. Hundt, M.; Sadler, P.; Levchenko, I.; Wolter, M.; Kersten, H.; Ostrikov, K. Real-time monitoring of nucleation-growth cycle of carbon nanoparticles in acetylene plasmas. *J. Appl. Phys.* **2011**, *109*, 123305. [CrossRef]
41. Zimmermann, S.; Ahner, N.; Blaschta, F.; Schaller, M.; Zimmermann, H.; Rülke, H.; Lang, N.; Röpcke, J.; Schulz, S.E.; Gessner, T. Influence of the additives Argon, O_2, C_4F_8, H_2, N_2 and CO on plasma conditions and process results during the etch of SiCOH in CF_4 plasma. *Microelectron. Eng.* **2011**, *88*, 671–676. [CrossRef]
42. Lang, N.; Hempel, F.; Strämke, S.; Röpcke, J. Time-resolved quantum cascade laser absorption spectroscopy of pulsed plasma assisted chemical vapor deposition processes containing BCl_3. *Jpn. J. Appl. Phys.* **2011**, *50*, 08JB04. [CrossRef]
43. Baby, A.; Mahony, C.M.O.; Maguire, P.D. Acetylene-argon plasmas measured at a biased substrate electrode for diamond-like carbon deposition: I. Mass spectrometry. *Plasma Sources. Sci. Technol.* **2011**, *20*, 015003. [CrossRef]
44. Guaitella, O.; Hübner, M.; Marinov, D.; Guerra, V.; Pintassilgo, C.D.; Welzel, S.; Röpcke, J.; Rousseau, A. Oxidation of NO into NO_2 by Surface Adsorbed O Atoms. *Contrib. Plasma Phys.* **2011**, *51*, 176–181. [CrossRef]
45. Welzel, S.; Guaitella, O.; Lazzaroni, C.; Pintassilgo, C.D.; Rousseau, A.; Röpcke, J. NO kinetics in pulsed low-pressure plasmas studied by time-resolved quantum cascade laser absorption spectroscopy. *J. Plasma Sources Sci. Technol.* **2011**, *20*, 015020. [CrossRef]
46. Marinov, D.; Lopatik, D.; Guaitella, O.; Hübner, M.; Ionikh, Y.; Röpcke, J.; Rousseau, A. Surface vibrational relaxation of N_2 studied by CO_2 titration with time-resolved quantum cascade laser absorption spectroscopy. *J. Phys. D Appl. Phys.* **2012**, *45*, 175201. [CrossRef]
47. Reuter, S.; Winter, J.; Iseni, S.; Peters, S.; Schmidt-Bleker, A.; Dünnbier, M.; Schäfer, J.; Foest, R.; Weltmann, K.-D. Detection of ozone in a MHz argon plasma bullet jet. *Plasma Sources Sci. Technol.* **2012**, *21*, 034015. [CrossRef]
48. Lopatik, D.; Niemietz, S.; Fröhlich, M.; Röpcke, J.; Kersten, H. Plasma Chemical Study of a RF Discharge Containing Aluminum Tri-Isoproxide Using MIR Absorption Spectroscopy Based on External-Cavity Quantum Cascade Lasers. *Contrib. Plasma Phys.* **2012**, *52*, 864–871. [CrossRef]
49. Lopatik, D.; Lang, N.; Macherius, U.; Zimmermann, H.; Röpcke, J. On the application of cw external cavity quantum cascade infrared lasers for plasma diagnostics. *Meas. Sci. Technol.* **2012**, *23*, 115501. [CrossRef]
50. Hübner, M.; Marinov, D.; Guaitella, O.; Rousseau, A.; Röpcke, J. On time resolved gas temperature measurements in a pulsed dc plasma using quantum cascade laser absorption spectroscopy. *Meas. Sci. Technol.* **2012**, *23*, 115602. [CrossRef]
51. Lopatik, D.; Marinov, D.; Guaitella, O.; Rousseau, A.; Röpcke, J. On the reactivity of plasma-treated photo-catalytic TiO_2 surfaces for oxidation of C_2H_2 and CO. *J. Phys. D Appl. Phys.* **2013**, *46*, 255203. [CrossRef]
52. Marinov, D.; Lopatik, D.; Guaitella, O.; Ionikh, Y.; Röpcke, J.; Rousseau, A. Surface deactivation of vibrationally excited N_2 studied using infrared titration combined with quantum cascade laser absorption spectroscopy. *J. Phys. D Appl. Phys.* **2014**, *47*, 015203. [CrossRef]
53. Yumii, T.; Kimura, N.; Hamaguchi, S. Quantum cascade laser absorption spectroscopy with the amplitude-to-time conversion technique for atmospheric-pressure plasmas. *J. Appl. Phys.* **2013**, *113*, 213101. [CrossRef]
54. Iseni, S.; Reuter, S.; Weltmann, K.-D. NO_2 dynamics of an Ar/Air plasma jet investigated by in situ quantum cascade laser spectroscopy at atmospheric pressure. *J. Phys. D Appl. Phys.* **2014**, *47*, 075203. [CrossRef]

55. Ouaras, K.; Delacqua, L.C.; Lombardi, G.; Röpcke, J.; Wartel, M.; Bonnin, X.; Redolfi, M.; Hassouni, K. In-situ diagnostics of hydrocarbon dusty plasmas using quantum cascade laser absorption spectroscopy and mass spectrometry. *J. Plasma Phys.* **2014**, *80*, 833–841. [CrossRef]
56. Reuter, S.; Winter, J.; Iséni, S.; Schmidt-Bleker, A.; Dünnbier, M.; Masur, K.; Wende, K.; Weltmann, K.-D. The influence of feed gas humidity versus ambient humidity on atmospheric pressure plasma jet-effluent chemistry and skin cell viability. *IEEE Trans. Plasmas Sci.* **2015**, *43*, 3185–3192. [CrossRef]
57. Bartlome, R.; de Wolf, S.; Demaurex, B.; Ballif, C.; Amanatides, E.; Mataras, D. Practical silicon deposition rules derived from silane monitoring during plasma-enhanced chemical vapor depositiona. *J. Appl. Phys.* **2015**, *117*, 203303. [CrossRef]
58. Lang, N.; Zimmermann, S.; Zimmermann, H.; Macherius, U.; Uhlig, B.; Schaller, M.; Schulz, S.E.; Röpcke, J. On treatment of ultra-low-k SiCOH in CF_4 plasmas: Correlation between the concentration of etching products and etching rate. *Appl. Phys. B* **2015**, *119*, 219–226. [CrossRef]
59. Hübner, M.; Lang, N.; Zimmermann, S.; Schulz, S.E.; Buchholtz, W.; Röpcke, J.; van Helden, J.H. Quantum cascade laser based monitoring of CF_2 radical concentration as a diagnostic tool of dielectric etching plasma processes. *Appl. Phys. Lett.* **2015**, *106*, 031102. [CrossRef]
60. Reuter, S.; Sousa, J.S.; Stancu, G.D.; van Helden, J.H. Review on VUV to MIR absorption spectroscopy of atmospheric pressure plasma jets. *Plasma Sources Sci. Technol.* **2015**, *24*, 054001. [CrossRef]
61. Van Gaens, W.; Iseni, S.; Schmidt-Bleker, A.; Weltmann, K.-D.; Reuter, S.; Bogaerts, A. Numerical analysis of the effect of nitrogen and oxygen admixtures on the chemistry of an argon plasma jet operating at atmospheric pressure. *New J. Phys.* **2015**, *17*, 033003. [CrossRef]
62. Hamann, S.; Börner, K.; Burlacov, I.; Spies, H.-J.; Röpcke, J. Spectroscopic investigations of plasma nitriding and nitrocarburizing processes using an active screen: A comparative plasma chemical study of two reactor types. *Contrib. Plasma Phys.* **2015**, *55*, 689–700. [CrossRef]
63. Hamann, S.; Börner, K.; Burlacov, I.; Spies, H.-J.; Strämke, M.; Strämke, S.; Röpcke, J. Plasma nitriding monitoring reactor: A model reactor for studying plasma nitriding processes using an active screen. *Rev. Sci. Instrum.* **2015**, *86*, 123503. [CrossRef] [PubMed]
64. Hübner, M.; Gorchakow, S.; Guaitella, O.; Marinov, D.; Rousseau, A.; Röpcke, J.; Loffhagen, D. Kinetic studies of NO formation in pulsed air-like low-pressure dc plasmas. *Plasma Sources Sci. Technol.* **2016**, *25*, 035005. [CrossRef]
65. Douat, C.; Hübner, S.; Engeln, R.; Benedikt, J. Production of nitric/nitrous oxide by an atmospheric pressure plasma jet. *Plasma Sources Sci. Technol.* **2016**, *25*, 025027. [CrossRef]
66. Nave, A.S.C.; Baudrillart, B.; Hamann, S.; Bénédic, F.; Lombardi, G.; Gicquel, A.; van Helden, J.H.; Röpcke, J. Spectroscopic study of low pressure, low temperature H_2-CH_4-CO_2 microwave plasmas used for large area deposition of nanocrystalline diamond films, Part I: On temperature determination and energetic aspects. *Plasma Sources Sci. Technol.* **2016**. submitted.
67. Nave, A.S.C.; Baudrillart, B.; Hamann, S.; Bénédic, F.; Lombardi, G.; Gicquel, A.; van Helden, J.H.; Röpcke, J. Spectroscopic study of low pressure, low temperature H_2-CH_4-CO_2 microwave plasmas used for large area deposition of nanocrystalline diamond films, Part II: On plasma chemical processes. *Plasma Sources Sci. Technol.* **2016**, submitted.
68. Nave, A.S.C.; Mitschker, F.; Awakowicz, P.; Röpcke, J. Spectroscopic studies of microwave plasmas containing hexamethyldisiloxane. *J. Phys. D Appl. Phys.* **2016**. submitted.
69. Namjou, K.; Cai, S.; Whittaker, E.A.; Faist, J.; Gmachl, C.; Capasso, F.; Sivco, D.L.; Cho, A.Y. Sensitive absorption spectroscopy with a room-temperature distributed-feedback quantum-cascade laser. *Opt. Lett.* **1998**, *23*, 219–221. [CrossRef] [PubMed]
70. Gmachl, C.; Capasso, F.; Sivco, D.L.; Cho, A.Y. Recent progress in quantum cascade lasers and applications. *Rep. Prog. Phys.* **2001**, *64*, 1533. [CrossRef]
71. Normand, E.; McCulloch, M.; Duxbury, G.; Langford, N. Fast, real-time spectrometer based on a pulsed quantum-cascade laser. *Opt. Lett.* **2003**, *28*, 16–18. [CrossRef] [PubMed]
72. Beyer, T.; Braun, M.; Lambrecht, A. Fast gas spectroscopy using pulsed quantum cascade lasers. *J. Appl. Phys.* **2003**, *93*, 3158–3160. [CrossRef]
73. Fischer, M.; Tuzon, B.; Hugi, A.; Brönnimann, R.; Kunz, A.; Blaser, S.; Rochat, M.; Landry, O.; Müller, A. Intermittent operation of QC-lasers for mid-IR spectroscopy with low heat dissipation: Tuning characteristics and driving electronics. *Opt. Express* **2014**, *22*, 7014–7027. [CrossRef] [PubMed]

74. Nelson, D.D.; McManus, J.B.; Urbanski, S.; Herndon, S.; Zahniser, M.S. High precision measurements of atmospheric nitrous oxide and methane using thermoelectrically cooled mid-infrared quantum cascade lasers and detectors. *Spectrochim. Acta A* **2004**, *60*, 3325–3335. [CrossRef] [PubMed]
75. McCulloch, M.T.; Normand, E.L.; Langford, N.; Duxbury, G.; Newnham, D.A. Highly sensitive detection of trace gases using the time-resolved frequency downchirp from pulsed quantum-cascade lasers. *J. Opt. Soc. Am. B* **2003**, *20*, 1761–1768. [CrossRef]
76. Kosterev, A.A.; Tittel, F.K.; Gmachl, C.; Capasso, F.; Sivco, D.L.; Baillargeon, J.N.; Hutchinson, A.L.; Cho, A.Y. Trace-gas detection in ambient air with a thermoelectrically cooled, pulsed quantum-cascade distributed feedback laser. *Appl. Opt.* **2000**, *39*, 6866–6872. [CrossRef] [PubMed]
77. Sonnenfroh, D.M.; Rawlins, W.T.; Allen, M.G.; Gmachl, C.; Capasso, F.; Hutchinson, A.L.; Sivco, D.L.; Baillargeon, J.N.; Cho, A.Y. Application of balanced detection to absorption measurements of trace gases with room-temperature, quasi-cw quantum-cascade lasers. *Appl. Opt.* **2001**, *40*, 812–820. [CrossRef] [PubMed]
78. McCulloch, M.T.; Duxbury, G.; Langford, N. Observation of saturation and rapid passage signals in the 10.25 micron spectrum of ethylene using a frequency chirped quantum cascade laser. *Mol. Phys.* **2006**, *104*, 2767–2779. [CrossRef]
79. Welzel, S.; Röpcke, J. Non-symmetrical line broadening effects using short-pulse QCL spectrometers as determined with sub-nanosecond time-resolution. *Appl. Phys. B* **2011**, *102*, 303–311. [CrossRef]
80. Capitelli, M.; Ferreira, C.M.; Gordiets, B.F.; Osipov, A.I. *Plasma Kinetics in Atmospheric Gases*; Springer: Berlin, Germany, 2000.
81. Röpcke, J.; Davies, P.B.; Hempel, F.; Lavrov, B.P. Emission and absorption spectroscopy. In *Low Temperature Plasmas—Fundamentals, Technologies and Techniques*, 2nd ed.; Hippler, R., Kersten, H., Schmidt, M., Schoenbach, K.H., Eds.; Wiley-VCH: Weinheim, Germany, 2008; Volume 1, pp. 215–242.
82. Allen, M.G. Diode laser absorption sensors for gas-dynamic and combustion flows. *Meas. Sci. Technol.* **1998**, *9*, 545. [CrossRef] [PubMed]
83. Q-MACSoft-HT. Available online: http://www.neoplas-control.de/ (accessed on 22 June 2016).
84. Rousseau, A.; Guaitella, O.; Röpcke, J.; Gatilova, L.V.; Tolmachev, Y.A. Combination of a pulsed microwave plasma with a catalyst for acetylene oxidation. *Appl. Phys. Lett.* **2004**, *85*, 2199–2201. [CrossRef]
85. Rousseau, A.; Gatilova, L.V.; Guaitella, O.; Guillard, C.; Thevenet, F.; Röpcke, J.; Stancu, G. Photocatalyst activation in a pulsed low pressure discharge. *Appl. Phys. Lett.* **2005**, *87*, 221501. [CrossRef]
86. Rousseau, A.; Meshchanov, A.V.; Röpcke, J. Evidence of plasma-catalyst synergy in a low-pressure discharge. *Appl. Phys. Lett.* **2006**, *88*, 021503. [CrossRef]
87. Guaitella, O.; Thevenet, F.; Guillard, C.; Rousseau, A. Dynamic of the plasma current amplitude in a barrier discharge: Influence of photocatalytic material. *J. Phys. D Appl. Phys.* **2006**, *39*, 2964. [CrossRef]
88. Guaitella, O.; Thevenet, F.; Puzenat, E.; Guillard, C.; Rousseau, A. C_2H_2 oxidation by plasma/TiO_2 combination: Influence of the porosity, and photocatalytic mechanisms under plasma exposure. *Appl. Catal. B* **2008**, *80*, 296–305. [CrossRef]
89. Guaitella, O.; Lazzaroni, C.; Marinov, D.; Rousseau, A. Evidence of atomic adsorption on TiO_2 under plasma exposure and related C_2H_2 surface reactivity. *Appl. Phys. Lett.* **2010**, *97*, 011502. [CrossRef]
90. Pintassilgo, C.D.; Guerra, V.; Guaitella, O.; Rousseau, A. Modelling of an afterglow plasma in air produced by a pulsed discharge. *Plasma Sources Sci. Technol.* **2010**, *19*, 055001. [CrossRef]
91. Van Gessel, A.F.H.; Alards, K.M.J.; Bruggemann, P.J. NO production in an RF plasma jet at atmospheric pressure. *J. Phys. D Appl. Phys.* **2013**, *46*, 265202. [CrossRef]
92. Daylight Solutions, User. Manual, Rev. A, 2009. Available online: www.daylightsolutions.com (accessed on 22 June 2016).